Available online at www.sciencedirect.com

SCIENCE DIRECT®

PALAEO

ELSEVIER

Palaeogeography, Palaeoclimatology, Palaeoecology 222 (2005) 344–369

www.elsevier.com/locate/palaeo

Late Glacial and Holocene paleoceanography in the Skagerrak from high-resolution grain size records

Richard Gyllencreutz*

Department of Geology and Geochemistry, Stockholm University, Sweden

Received 3 November 2004; received in revised form 5 January 2005; accepted 21 March 2005

Abstract

High-resolution grain size analyses of the AMS ^{14}C-dated, 32 m long core MD99-2286 from the northeastern Skagerrak were performed in order to study late Glacial and Holocene paleoceanographic and sedimentary changes. All ages in this study are given in calibrated thousand years before present (= AD 1950), abbreviated 'kyr', unless otherwise noted.

The distinct ending of IRD (ice rafted debris) in core MD99-2286, which was retrieved from a location down current from the final calving ice margin in the region, indicates that iceberg calving in the Skagerrak ended between 10.6 and 10.2 kyr.

A clay-rich sequence in core MD99-2286, deposited between 11.3 and 10.3 kyr, is attributed to outflow from the Baltic basin across south central Sweden. The sequence is correlated to similar units from cores along the Swedish west coast. The onset of this clay-rich deposition occurs progressively later in cores further south along the coast, supporting a previous hypothesis that differential glacio-isostatic uplift caused a southward migration of the Baltic outflow from the Otteid-Stenselva to the Göta Älv outlet.

A distinct coarsening towards younger sediments in core MD99-2286 indicates a hydrographic shift at 8.5 kyr, which is correlated to a shift previously reported in the Skagerrak, Kattegat and the Norwegian Channel. This shift reflects the establishment of the modern circulation system in the eastern North Sea, as a consequence of the opening of the English Channel and the Danish straits and increased Atlantic water inflow, and the subsequent development of the South Jutland Current. A general trend of coarsening, poorer sorting and increasing variability from 8.5 kyr until the present indicates increasing strength and influence of the variable South Jutland Current.

A series of changes from ca. 6.3 to ca. 3.8 kyr in core MD99-2286 reflects strengthening of the Jutland Current towards the present day sedimentation system in the Skagerrak–Kattegat. These changes are correlated to previously reported hydrographic shifts at 5.5 ^{14}C years BP in the Skagerrak and at 4.0 ^{14}C years BP in the Kattegat. It is suggested that these shifts were separate features of a transitional period related to strengthening of the current system. The resulting changes are differently manifested in different parts of the Skagerrak–Kattegat, due to the complex circulation system.

* Tel.: +46 709 62 54 09; fax: +46 8 674 78 97.
E-mail address: richard.gyllencreutz@geo.su.se.

doi:10.1016/j.palaeo.2005.03.025

The last 800 years are characterised by poorly sorted sediments with a relatively high and variable proportion of coarse material, reflecting a circulation system significantly modified by regional climatic conditions, especially the general wind directions and storm frequency over the southern North Sea.

Keywords: Skagerrak; Holocene; grain size; sediment; Baltic Sea; hydrographic shift

1. Introduction

The Skagerrak is the major sink for fine-grained matter in the North Sea, and thus is a target area for studies of the latest Pleistocene and Holocene oceanographic and climatic history of the North Sea region, including adjacent land areas. The circulation and subsequent sedimentation in the Skagerrak is mainly driven by the North Atlantic Current, with important contributions from the Jutland Current and minor contributions from Baltic Sea outflow and continental runoff predominantly from the Scandinavian countries (Longva and Thorsnes, 1997). This system was developed during early Holocene times following the deglaciation.

The spatial distribution of textural provinces in the Skagerrak is well known from numerous investigations during the last 20 years (van Weering, 1981; Fält, 1982; van Weering et al., 1987, 1993; Kuijpers et al., 1993; Pederstad et al., 1993; North Sea Task Force, 1993) including the study of 268 short (< 0.5 m) cores from the Norwegian part of the Skagerrak (Stevens et al., 1996; Bøe et al., 1996, Ottesen et al., 1997). Previous grain size investigations of cores longer than 2 m comprise eight cores for which age models have been published (Björklund et al., 1985; Hass, 1996; Bergsten, 1994; Senneset, 2002), including the 220 m long Skagen 3/4 core, drilled onshore in northernmost Denmark (Knudsen et al., 1996; Conradsen and Heier-Nielsen, 1995; Jiang et al., 1997) and at least 11 cores lacking age models (Cato et al., 1982; van Weering, 1982a). The sedimentation in the Skagerrak has been addressed in several special volumes (Longva and Thorsnes, 1997; Bøe and Thorsnes, 1996; Liebezeit et al., 1993; Stabell and Thiede, 1985) and was comprehensively reviewed by van Weering et al. (1993). These efforts demonstrate that there are a limited number of high-resolution studies (decadal or better) of long Skagerrak cores having accurate chronostratigraphic control.

Several studies focused on transport mechanisms and source areas have shown that the sediments in northeastern Skagerrak are mainly deposited from suspension, consisting of a mixture of material derived from the North Sea/Atlantic Ocean, Scandinavia/Baltic Sea and reworked material from mainly the southern North Sea (van Weering, 1981; Eisma and Kalf, 1987; Eisma and Irion, 1988; Kuijpers et al., 1993; van Weering et al., 1993; Rodhe and Holt, 1996; Longva and Thorsnes, 1997).

The present study investigates sedimentation and paleocurrent variability throughout the late Glacial and the Holocene, using detailed grain size analysis from the 32 m long core MD99-2286 retrieved from the position 58.7381°N, 10.2055°E in the northeastern Skagerrak at 225 m water depth (Labeyrie et al., 2003; Gyllencreutz et al., 2005).

2. Oceanographic and sedimentary setting

The Skagerrak is bordered by the coasts of Denmark, Sweden and Norway, and consists of a sedimentary basin that forms the inner end of the Norwegian Trench (Fig. 1). The water depths in the Skagerrak exceed 700 m, making it the deepest part of the otherwise relatively shallow North Sea (average water depth is 94 m; Svansson, 1975). The present large-scale circulation in the Skagerrak (Fig. 1) has been described by Svansson (1975), Rodhe (1987, 1996, 1998) and reviewed by Otto et al. (1990). The circulation and subsequent sedimentation in the Skagerrak is mainly governed by the North Atlantic Current, through water entering the North Sea between Scotland and Norway in the north and via the English Channel in the southwest. Southern North Sea Water is mixed with English Channel water and relatively small amounts of low salinity river outflow, and the mixed waters continue as the variable Jutland Current (Danielssen et al.,

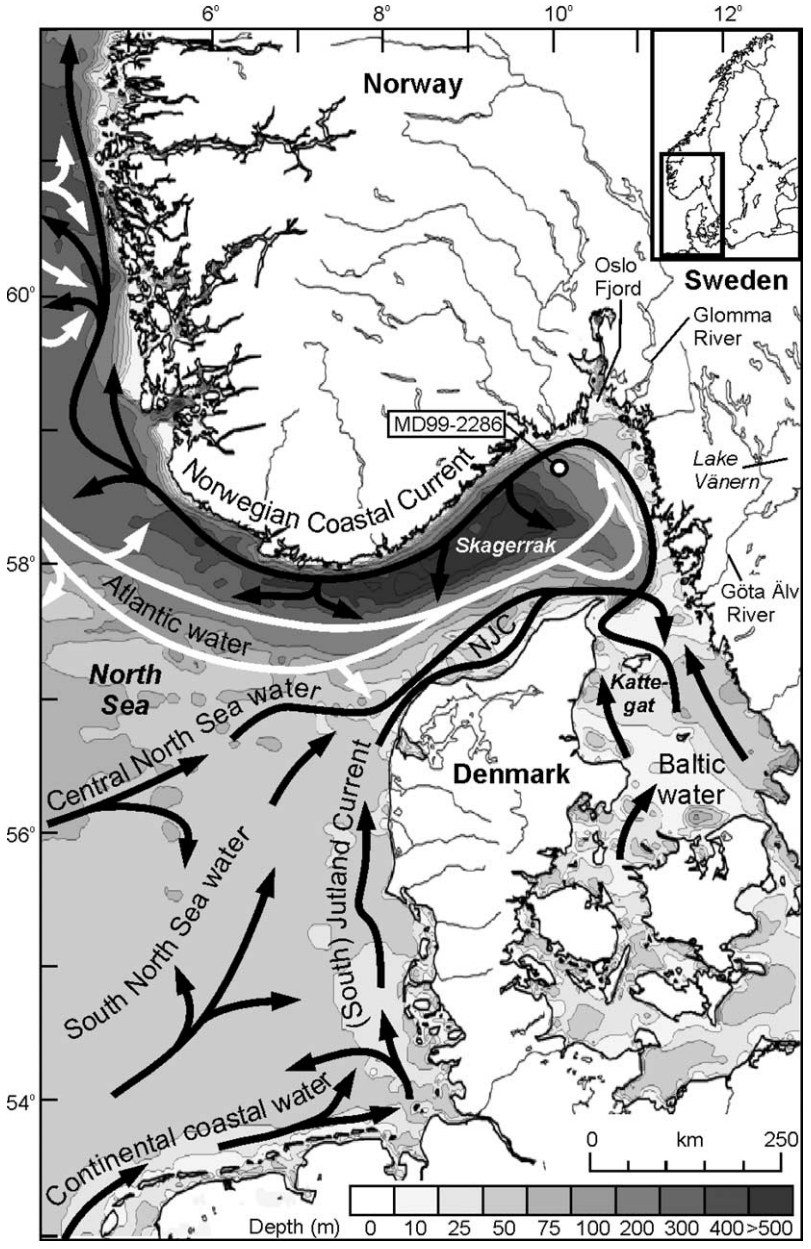

Fig. 1. Bathymetry and general ocean circulation (arrows) in the eastern North Sea and the Skagerrak. White arrows mark the part of Atlantic water, which flows more or less directly into the Skagerrak. NJC=North Jutland Current. The location of core MD99-2286 is marked with a circle. Current pattern modified from Longva and Thorsnes (1997). Bathymetry from the ETOPO2 database (Smith and Sandwell, 1997).

1997, Longva and Thorsnes, 1997) along the Danish west coast towards the Skagerrak. As the Jutland Current moves further to the northeast, it mixes with the Central North Sea Water and with fresher and colder outflow waters from the Baltic Sea. This mixed current makes a cyclonic turn in the north-eastern end of the Skagerrak, where the water depth increases and the current speed is reduced beyond the limit where the intensity of turbulence can support a steady concentration of suspended matter

(Rodhe and Holt, 1996). As a result, fine-grained sediments are deposited at a high relative rate, up to 1 cm/year, in the northeastern and central parts of the Skagerrak (van Weering, 1982a; Bøe et al., 1996). After the cyclonic turn the current continues as the Norwegian Coastal Current, following the Norwegian trench to the southwest, where the current exits the Skagerrak and continues north along the coast of Norway.

Most of the suspended sediment entering the Skagerrak originates from inflowing Atlantic water with a low sediment concentration (Longva and Thorsnes, 1997), with important contributions from the Jutland Current, carrying a high sediment load of erosional products from the coasts of Jutland (Eisma and Kalf, 1987). Rivers are small contributors (Kuijpers et al., 1993; Pederstad et al., 1993).

Literature describes a series of major paleoenvironmental changes in the Skagerrak during the late Pleistocene and the Holocene. These changes include the deglaciation of the region (1), freshwater outflow from the Baltic basin (2), paleogeographic changes (3), opening of the English Channel and a connection to the Baltic Sea in southern Kattegat (4), and a hydrographic shift during mid-Holocene times (5).

1. The complicated deglaciation history of the outer Oslo Fjord and the northeastern Skagerrak has been described by, e.g., Lundqvist and Wohlfarth (2001), Andersen et al. (1995), Sørensen (1979, 1992), Berglund (1979) and Mörner (1979). Directly after the deglaciation of the MD99-2286 coring site between ca. 14.5 and 13.6 kyr (Gyllencreutz et al., 2005), the Skagerrak was a fjord-like basin, bordered to the south by large land areas west of Denmark (Stabell and Thiede, 1986; Thiede, 1987).
2. The Skagerrak was subjected to a major fresh water input from the final drainage of the Baltic Ice Lake (BIL) at ca. 11.6 kyr (Björck, 1995; Andrén et al., 2002; Björck et al., 2002). A few hundred years later, the Närke Strait in south central Sweden opened (Björck, 1995; Lambeck, 1999), allowing fresh water from the Baltic to enter the Skagerrak through outlets along the Swedish west coast. This flow ceased when the outlets across Sweden were closed due to glacio-isostatic uplift around 10.3 kyr (Table 1, event f) (Björck, 1995; Lambeck, 1995).

Table 1
Calibration of ^{14}C dates of discussed events in the Skagerrak–Kattegat

Interpreted event	Reference	^{14}C age (ka BP)	Cal. age (kyr)
(a) Transgression of s. North Sea	Stabell and Thiede, 1986; Lambeck, 1995	10	11.6–11.3
(b) End of IRD dep. in Skagerrak	van Weering, 1982a,b	10	11.6–11.3
(c) Aker IMZ, Oslo area	Andersen et al., 1995; Gjessing, 1980; Gjessing and Spjeldnaes, 1979; Sørensen, 1979	9.8–9.6	11.3–10.8
(d) Marine limit, Oslo area	Hafsten, 1983	9.7	11.2–10.8
(e) Glomma drainage event	Longva and Bakkejord, 1990; Longva and Thoresen, 1991	9.1	10.4–10.2
(f) Otteid-Stenselva strait closing	Lambeck, 1999; Björck, 1995	9.1	10.4–10.2
(g) English Channel opening	Nordberg, 1991	8	9.0–8.7
(h) English Channel opening	Conradsen and Heier-Nielsen, 1995	7.6	8.5[a]
(i) English Channel opening	Jiang et al., 1997	7.7	8.6[a]
(j) English Channel opening	Björklund et al., 1985	8–7	9.0–7.7
(k) English Channel opening	Lambeck, 1995; Jelgersma, 1979	8–7	9.0–7.7
(l) Danish straits opening	Björck, 1995	8.2	9.3–9.0
(m) Danish straits opening	Conradsen, 1995	8	9.0–8.7
(n) Danish straits opening	Lambeck, 1999	7.5–7.8	8.7–8.2
(o) Isolation of Dogger Bank	Lambeck, 1995	8	9.0–8.7
(p) S–K hydrographic shift	Conradsen, 1995; Conradsen and Heier-Nielsen, 1995	5.5	6.2[a]
(q) S–K hydrographic shift	Jiang et al., 1997	5.1	5.9[a]
(r) S–K hydrographic shift	Nordberg, 1991; Nordberg and Bergsten, 1988	4	4.6–4.3

The ages were calibrated using cited (reservoir corrected) ^{14}C ages with an assumed uncertainty of ± 100 years, using the calibration data set INTCAL98 (Stuiver et al., 1998a). Results are given in kyr as 1σ ranges rounded to hundreds of years.

[a] Calibrated ages inferred from the Conradsen and Heier-Nielsen (1995) age model using calibrated ages by Petersen (2004).

3. A major geographic change of the southern coastlines of the Skagerrak began at about 11.6–11.3 kyr (Table 1, event a) when the transgressing North Sea advanced into the former land region west of Jutland (Stabell and Thiede, 1986; Lambeck, 1995). The continuing transgression allowed water flow south of the Dogger Bank shortly after 9–8.7 kyr (Table 1, event o) (Lambeck, 1995).
4. The English Channel opened at about 9–7.7 kyr (Lambeck, 1995; Jelgersma, 1979). Nordberg (1991) argued that the opening of the English Channel was prerequisite for the formation of the South Jutland Current and the Norwegian Coastal Current. Stratigraphic data from the Skagerrak and the Kattegat indicate a major hydrographic shift reported between 9 and 7.7 kyr (Table 1, events g–k), interpreted as an effect of the opening of the English Channel (Jiang et al., 1997; Conradsen and Heier-Nielsen, 1995; Nordberg, 1991; Nordberg and Bergsten, 1988, Björklund et al., 1985). Fresh water from the Baltic has entered the Skagerrak via southern Kattegat since the opening of the Danish straits around 9.3–8.2 kyr (Table 1, events l and n) (Lambeck, 1999; Björck, 1995).
5. Studies of cores from the Skagerrak and the Kattegat indicate that the modern circulation system was established in conjunction with a hydrographic shift, reported at various ages between 4.3 and 6.2 kyr (Table 1, events p–r) (Jiang et al., 1997; Conradsen and Heier-Nielsen, 1995; Conradsen, 1995; Nordberg, 1991; Nordberg and Bergsten, 1988). This shift was synchronous with the final drowning of the Jutland Bank (Leth, 1996), and is marked by an increased flow of the Jutland Current and enhanced saline inflow to the Skagerrak and the Kattegat from the North Sea (Jiang et al., 1997; Conradsen and Heier-Nielsen, 1995; Conradsen, 1995; Nordberg, 1991).

3. Methods

3.1. Age convention: calibrated years BP versus ^{14}C years BP

All ages will hereafter be given in calibrated thousand years before present (= AD 1950), abbreviated 'kyr'. The increasing use of calibrated ages and the improved calibration data sets (Stuiver et al., 1998a,b) advocate the use of a calibrated age scale to facilitate comparison of the present results with other records of various origins. ^{14}C ages for discussed events from the literature were calibrated with an assumed uncertainty of ± 100 years, using the calibration data set INTCAL98 (Stuiver et al., 1998a), and has been summarised in Table 1. This approach does not qualify as a strict calibration in the technical sense, but is used to get a meaningful general picture of the course of events.

3.2. Carbonate correction

Carbonate was not removed from the samples, but the carbonate content in core MD99-2286 was measured on a UIC Coulometrics coulometer. The sampling interval was 10 cm from 15 to 32.4 m, 5 cm from 0 to15 m and 2 cm from 1 to 2.5 m. Analyses were performed on 60 mg of milled, freeze-dried bulk sediment samples. The results from the coulometer given in % carbonate–carbon were stoichiometrically re-calculated to % $CaCO_3$. The carbonate data were calibrated using a regression based on measurements of pure $CaCO_3$ (*Pro Analysi*) on 88 samples, with a standard deviation of 0.76% $CaCO_3$.

The effect of carbonate content on the particle size distribution was tested by linear regressions through carbonate content versus all grain size parameters discussed in this paper, respectively. The linear regressions show that carbonate is positively correlated to fine silt (2–10 μm), yielding $R^2=0.50$, but is poorly correlated to all other grain size parameters and explains little of the grain size variance (R^2-values range between 0.02 and 0.11). A minor exception to this is clay content (%<2 μm), which shows a strong negative correlation to carbonate content ($R^2=0.86$) in a short interval between 3070 and 3150 cm, equivalent to 11.16–10.17 kyr.

3.3. Grain size analysis

Sampling resolution for the grain size analysis was 5 cm in the core depth interval 0–1500 cm and 3100–3200 cm, and 10 cm in the interval 1500–3100 cm. De-ionized water saturated with pure calcium carbonate (*Pro Analysi*) was used as dispersing liquid throughout the grain size analysis, in order to prevent

dissolution of carbonate in the sediment. Between 2.5 and 3 g of freeze-dried sediment were suspended on a shaker-table overnight and was then wet-sieved using 63 μm mesh size. The coarse fraction was oven dried at 70 °C overnight and weighed after cooling to room temperature. The < 63 μm fine fraction samples were analyzed using a Sedigraph 5100 supplied with a Micromeritics MasterTech 051 automatic sample-

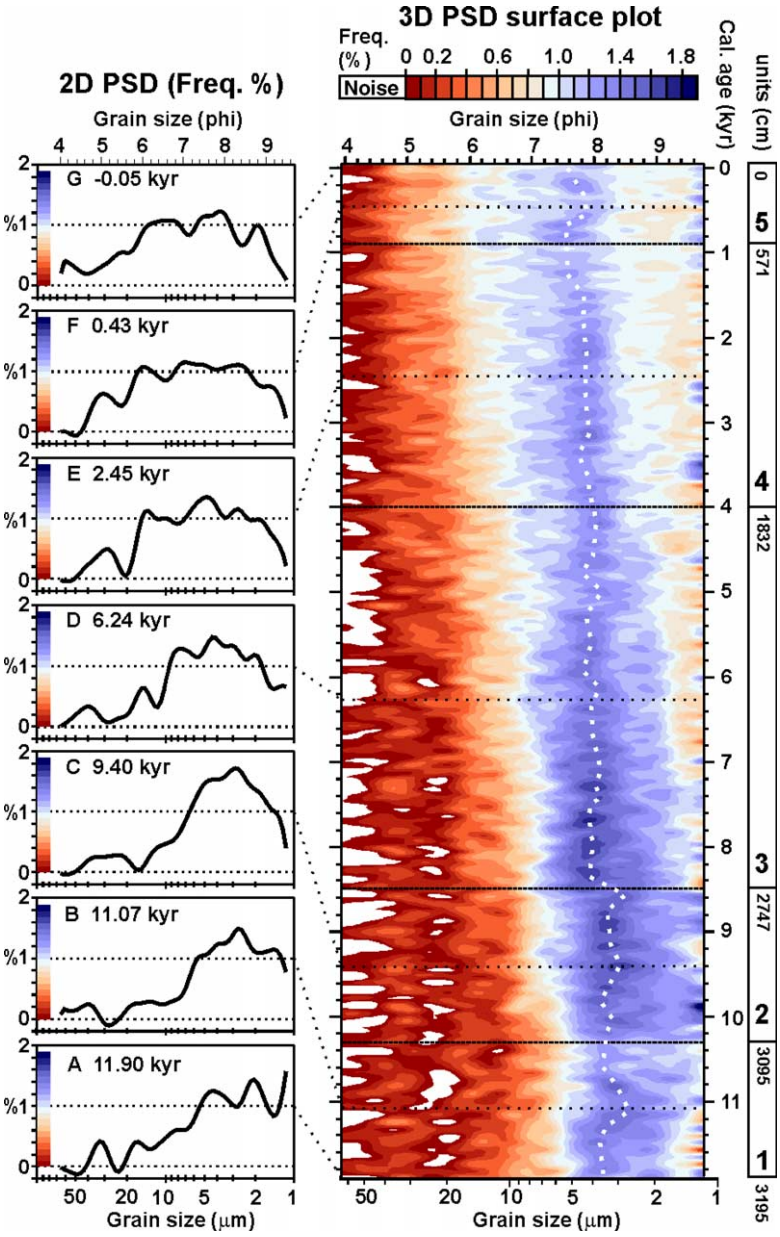

Fig. 2. 3D PSD surface plot of grain size variations with age in core MD99-2286 (right), and discrete plots of log-normal 2D PSDs for representative samples from the middle of each defined lithological unit and from the top and bottom of the core (left). The lithological units (far right) are defined in Fig. 5. The 2D plots can be viewed as 'slices' through the 3D PSD surface plot. The values below 0% (lower dotted line) in the 2D PSD diagrams correspond to the noise-affected regions (white) in the PSD surface plot. The visually estimated position of the grain size mode is marked by the white dotted line in the 3D PSD surface plot.

handling device. The sedigraph technique is described in detail in Coakley and Syvitski (1991). The sedigraph was set to measure grain sizes between 63 μm and 1 μm using the 'standard' analysis type, sample material set to 'glass' with a density of 2.615 g/cm^3 and analysis liquid set to 'water'. Sedigraph samples were analyzed in batches of 10 and the sample order was randomized within each batch. Prior to the sedigraph analysis, the centrifuged samples were resuspended using an ultra sonic bath and a vortex tube, and were agitated using an ultra sonic probe for 30 s. All coarse fraction samples from 3060 cm core depth and downward were visually studied for composition and grain size using a reflectance microscope, with an ocular-scale calibrated to a precision of 0.1 mm at the magnification used.

3.4. Grain size visualization

Conventional use of sediment grain size data for paleoenvironmental reconstructions is usually restricted to simple statistical descriptions of the particle size distribution (PSD), such as mode, mean, standard deviation, skewness and kurtosis. These descriptive parameters can serve as proxies for generalized down-core variability in depositional conditions and processes, but are not sensitive to open-ended, polymodal or non-normal distributions. In this study, the raw grain size data is visualized in its entirety in the form of three-dimensional PSD surface plots (Beierle et al., 2002), providing down-core continuity with preserved sample-level detail (Fig. 2).

Grain size measurements were automatically recorded by the sedigraph software in 250 size intervals set to range from 63 to 1 μm, expressed as cumulative-mass percent of equivalent spherical diameter. The sedigraph data was corrected for the coarse fraction removed through sieving, by multiplying all cumulative values with the weight percentage of the < 63 μm fraction for each sample. The data used for the PSD surface plot was gridded using the "Nearest Neighbour" method, with 5-cm resolution in order to avoid data loss from under-sampling, and the output grid model was smoothed using a 9 × 9 term

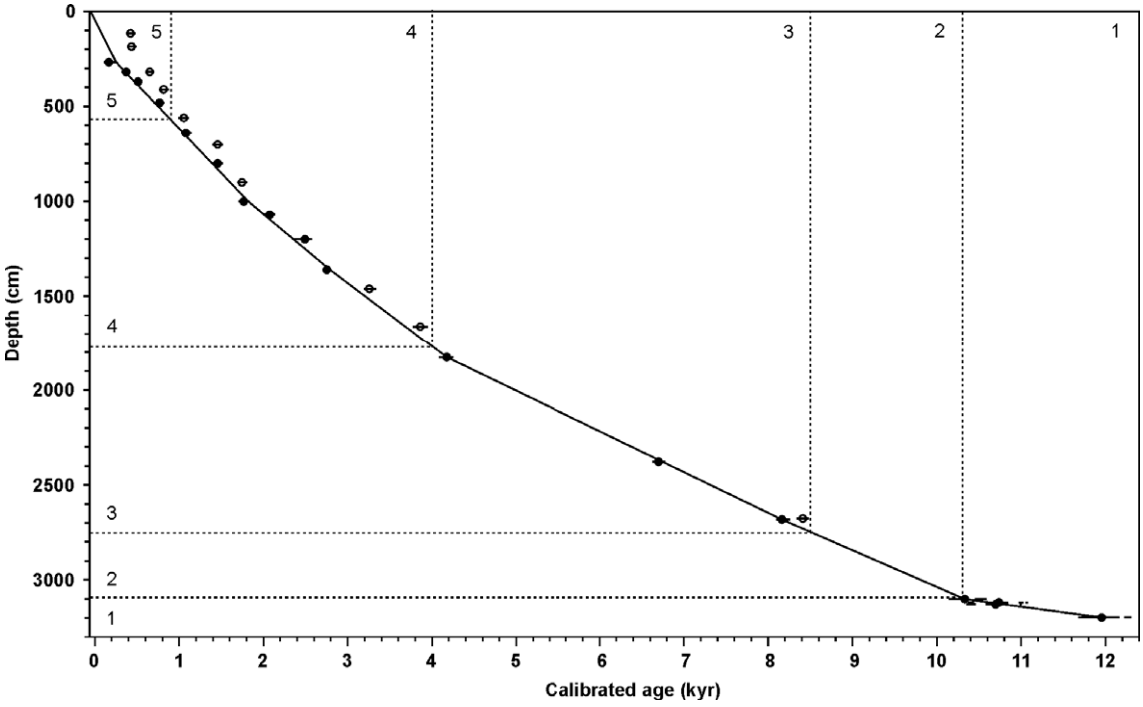

Fig. 3. Age model for core MD99-2286 based on 27 AMS ^{14}C dates. The age model is shown with a line connecting filled circles. Open circles show age estimates excluded from the age model because of presumed sediment reworking. Error bars (horizontal lines through the dates) denote 1σ calibrated age ranges (see also Table 2). The depths and ages of the lithological unit boundaries are marked with dotted lines.

Table 2
AMS ^{14}C dating of core MD99-2286

Laboratory reference	Corr. depth[a]	Nominal depth	$\delta^{13}C$ vs. PDB		^{14}C age (Libby h.l.)		Age range (cal. years BP) probability method			Dated species	Weight	Type[b]
	(cm)	(cm)	(‰)	±1σ	(C-14 years BP)	±1σ	Max (1σ)	Median	Min (1σ)		(mg)	
(ETH-24953)	115.5	115.5	− 3.8	1.2	785	50	480	424	378	*Scaphander* sp.	27.78	g,w
(ETH-25546)	185.5	185.5	2.0	1.2	800	55	494	436	393	*Yoldiella lucida*	8.85	m,w
ETH-24001	268	268	1.7	1.2	535	50	252	166	113	*Ennucula tenuis*	26.1	m,w
ETH-24397	319.5	319.5	1.8	1.2	730	45	417	372	320	*Thyasira equalis*	49.67	m,b
(ETH-26937)	319.5	319.5	0.5	1.2	1095	55	701	652	613	Foraminifera (mixed fauna)	11.86	f
ETH-25547	370.5	370.5	0.7	1.2	900	60	548	513	467	*Nucula tumidula*	9.55	m,b
(ETH-26388)	410.5	410.5	0.1	1.2	1270	50	877	814	761	Foraminifera (mixed fauna)	13.07	f
ETH-26938	481.5	481.5	2.7	1.2	1225	55	824	768	699	Foraminifera (mixed fauna)	16.77	f
(ETH-26939)	561	561	− 0.1	1.2	1510	50	1115	1057	992	Foraminifera (mixed fauna)	18.57	f
ETH-26940	640.5	640.5	0.8	1.2	1530	50	1146	1080	1024	Foraminifera (mixed fauna)	16.23	f
(ETH-25955)	700.5	700.5	2.3	1.2	1915	55	1518	1458	1398	Foraminifera (mixed fauna)	16.42	f
ETH-25956	801	801	−0.2	1.2	1915	55	1518	1458	1398	Foraminifera (mixed fauna)	18.04	f
(ETH-26389)	901	901	0.5	1.2	2155	50	1808	1744	1690	Foraminifera (mixed fauna)	19.29	f
ETH-26390	1001	1001	− 0.5	1.2	2175	50	1819	1766	1705	Foraminifera (mixed fauna)	15.51	f
ETH-26941	1070.5	1070.5	3.0	1.2	2440	55	2138	2076	1997	Foraminifera (mixed fauna)	11.62	f
ETH-26418	1200.5	1200.5	1.4	1.2	2765	60	2572	2493	2360	Foraminifera (mixed fauna)	12.56	f
ETH-27241	1360.5	1400.5	0.0	1.2	2975	55	2789	2752	2704	Foraminifera (mixed fauna)	14.87	f
(ETH-26419)	1460.5	1500.5	1.3	1.2	3390	60	3334	3256	3192	Foraminifera (mixed fauna)	14.05	f
(ETH-27242)	1660.5	1700.5	− 1.7	1.2	3895	60	3952	3861	3775	Foraminifera (mixed fauna)	18.1	f
ETH-26137	1826	1866	1.0	1.2	4120	60	4252	4173	4081	*Polinices montagui*	16.73	g,w
ETH-24003	2377	2417	1.3	1.2	6255	65	6773	6698	6628	*Portlandia intermedia*	42.6	m,b
ETH-25548	2676.5	2716.5	3.4	1.2	7955	70	8478	8410	8335	*Pseudamusium septemradiatum*	62.37	m,b
(ETH-25549)	2681.5	2721.5	2.9	1.2	7710	60	8262	8163	8099	*Pseudamusium septemradiatum*	100.02	m,b
ETH-25550	3100.5	3140.5	− 0.6	1.2	9620	70	10,585	10,332	10,145	*Pseudamusium septemradiatum*	44.68	m,b
ETH-24004	3119	3159	1.1	1.2	9955	85	11,080	10,734	10,373	*Bathyarca glacialis*	25.5	m,b
ETH-25551	3129.5	3169.5	− 2.0	1.2	9910	70	11,003	10,696	10,354	*Cryptonautica affinis*	25.77	g,b
ETH-24005	3198	3238	1.4	1.2	10,715	80	12,306	11,954	11,678	*Portlandia intermedia*	134.5	m,b

Laboratory reference codes in parentheses denote samples omitted from the age model due to presumed sediment reworking.

[a] Correction for artificial void in core at 1315–1355 cm; nominal depths below 1355 cm are reduced by 40 cm.

[b] Type abbreviations: g=gastropod, m=mollusc, f=benthic foraminifera, w=whole, b=broken.

2D Gaussian filter. A grey-scale PSD surface plot smoothed with three runs of the same filter was made as a schematic visual aid using the same data set.

The mode was visually estimated from the PSD surface plot, by connecting the highest points of the main modal ridge (dotted white line in Fig. 2). Median grain size was linearly interpolated from the two values closest to 50% in the cumulative distribution of each sample. Sortable silt median size was calculated in the same way after normalising the size fractions in the 10–63 μm interval to 100%.

3.5. Dating

The age model for core MD99-2286 is based on 27 AMS ^{14}C dates from samples of either mollusk shells of known species or mixed benthic foraminifera. The radiocarbon dates were calibrated using the CALIB

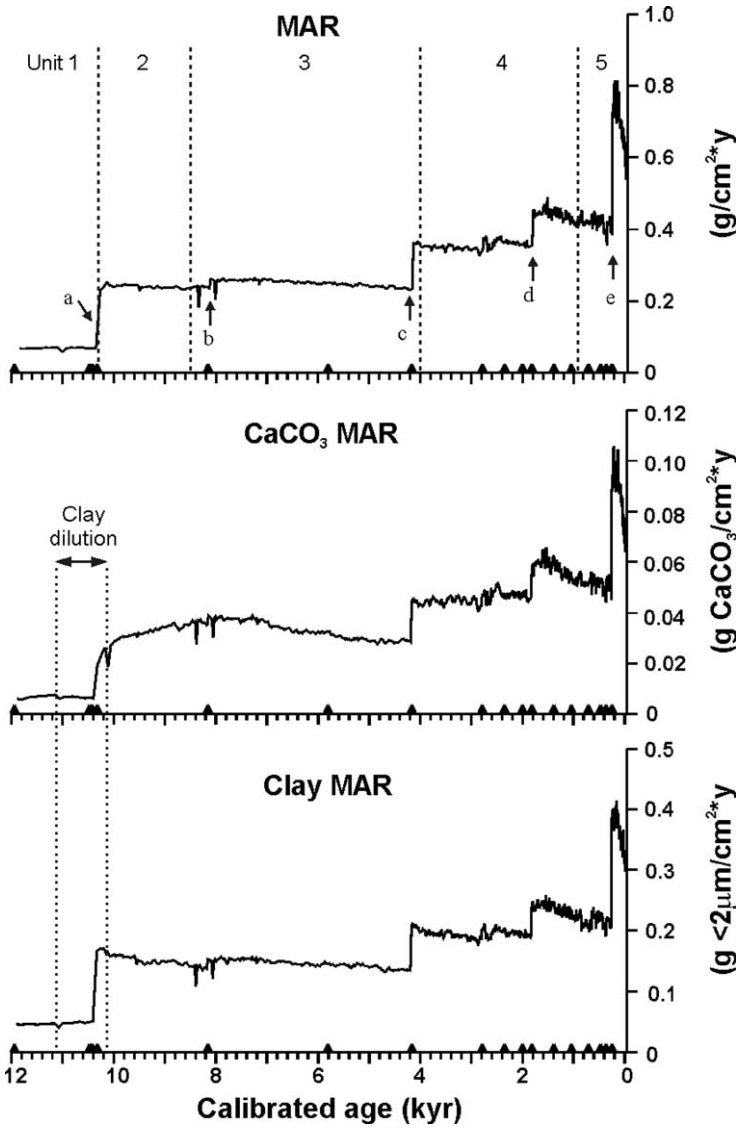

Fig. 4. MAR, $CaCO_3$ MAR and clay MAR in core MD99-2286. Black triangles on the age scale denote age control points. Dashed vertical lines in the MAR plot mark grain size unit boundaries. The major changes in MAR are marked with letters a–e. The interval with increased clay content (see also Fig. 5) is indicated with dotted vertical lines in the $CaCO_3$ MAR and clay MAR plots.

(rev 4.4) software (Stuiver and Reimer, 1993), which present the calibrated ages based on the probability method (Telford et al., 2004). The samples were assumed to consist of 100% marine carbon and the calibration data set MARINE98 (Stuiver et al., 1998b) was used. In order to facilitate comparison with other studies, a standard reservoir correction of 400 years was used for all samples, although it is recognized that the reservoir age may have been greater during the deglaciation (Bard et al., 1990; Bondevik et al., 1999). Calibration of published radiocarbon dates for the previous core Solberga-2 (Bodén et al., 1997) was performed using the same method, and the results are further described in the discussion below. The age model for core MD99-2286 is shown with defined lithological units in Fig. 3, and the dating and calibration results are shown in Table 2. The results of the dating, calibration and age model were discussed by Gyllencreutz et al. (2005).

3.6. Mass Accumulation Rate (MAR)

MAR is calculated as the product of linear sedimentation rate and dry (bulk) density. Clay and carbonate MARs are calculated as the product of MAR and the weight fraction of each parameter (clay or carbonate). Dry density values were obtained from sample bulk mass and whole-core GRA-density measurements performed with 2-cm resolution onboard *R/V Marion Dufresne* using a GeoTek Multi Sensor Core Logger (MSCL). The details of the MSCL measurements are given in Gyllencreutz et al. (2005). The linear sedimentation rate was calculated from the age model. The MAR, clay MAR and $CaCO_3$ MAR curves are shown in Fig. 4.

4. Results

4.1. MAR

The lowest MARs in the core are recorded in the bottom of unit 1 and the MAR generally increases through the entire record (Fig. 4). The step-like major increases in the MAR curve are caused by the change of slope at the inflection-points of the age model. However, the real changes in linear sedimentation rate are more likely to occur gradually somewhere between the control-points, and not abruptly at the dated levels. The major changes in MAR are marked with letters in Fig. 4.

4.2. Grain size

4.2.1. Choice of grain size parameters

The interpretation of the MD99-2286 grain size record is based on the entire particle size distribution (Fig. 2), and the discrete parameters clay content, fine silt content, sortable silt median, sortable silt content, coarse fraction content and median grain size. Clay (< 2 μm) and fine silt (2–10 μm) are used because they are the major components of the sediment in core MD99-2286. The sortable silt median is a proxy for relative current speed (McCave et al., 1995), whereas the sortable silt content is used for quality control of the sortable silt median. The coarse fraction (> 63 μm) content is very low (0.1–1%), and is used for interpretation of IRD deposition and as an additional current strength indicator. The median grain size is used as a statistical measure of central tendency and reflects the major grain size variations.

4.2.2. Lithological sub-division rationale

The core has been sub-divided into five units based on grain size variations. The median grain size was chosen as the base for the unit definition because it reflects major changes observed in most of the individual grain size parameters. The boundaries were thus defined in the mid-points of distinct increases in the grain size median, except the boundary between units 1 and 2, which is defined at the highest peak in clay content, because the median grain size is below the set detection limit (1 μm) in this part of the record. The features used for the boundary definitions are marked with arrows and roman numerals in Fig. 5. The characteristics of the units, labelled 1–5 from oldest to youngest, are described below.

4.2.3. General remarks on the grain size record

The PSD surface plot (Fig. 2) shows a relatively flat and/or polymodal grain size distribution, indicative of poorly sorted material in the entire core. The plot shows a trend of flattening in younger sediments, seen as slightly diverging frequency contours (Fig. 2), indicating that sorting decreases with time.

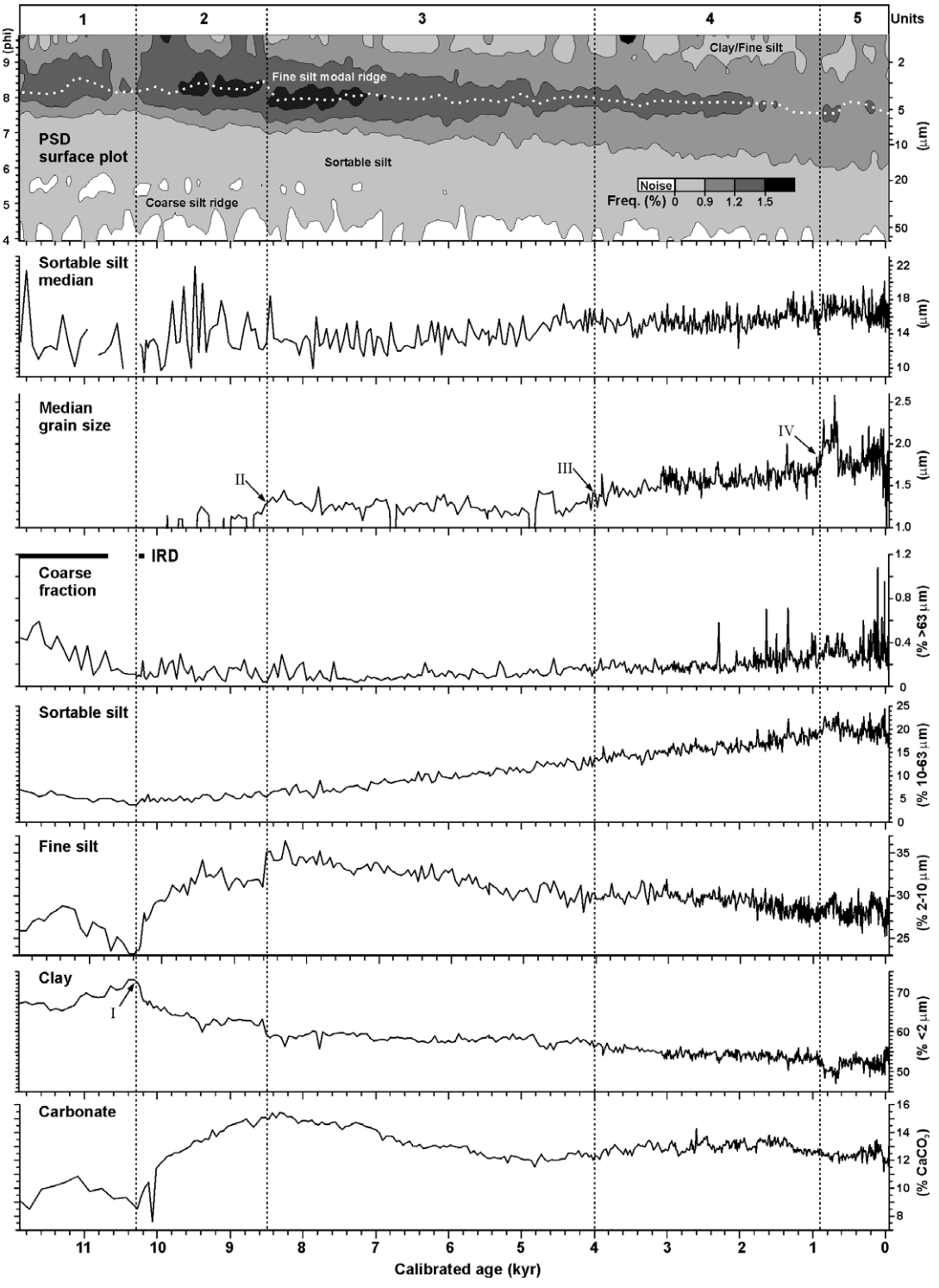
1
2
3
4
5
Units
(phi)
Clay/Fine silt
Fine silt modal ridge
PSD
surface plot
Sortable silt
Coarse silt ridge
Noise
Freq. (%) 0 0.9 1.2 1.5
(μm)
Sortable silt
median
Median
grain size
II
III
IV
IRD
Coarse
fraction
(% >63 μm)
Sortable silt
(% 10-63 μm)
Fine silt
(% 2-10 μm)
Clay
I
(% <2 μm)
Carbonate
(% CaCO3)
Calibrated age (kyr)

Due to the markedly small amounts of coarse material, the signal to noise ratio is very low in the coarse end of the PSD surface plot. The noise appears as negative percentages, visualized in Fig. 2 as blank regions occurring in the coarse end of the PSD. The noisy size interval is broadest in the oldest part of the core and narrows gradually towards the younger parts. All percentages within the size intervals where negative values occur are probably affected by noise and should be read as close to zero (Giancarlo Bianchi, Cardiff University, August 2003, personal comm.). Therefore, the negative values are shown with white colour in the PSD surface plot, and all values within the noise-affected size interval were rejected in the calculation of median and sortable silt median.

The total sum of the percentages for each sample in the surface plot varies between ca. 40% and 60%, as the remaining material consists of clay finer than 1 μm, which is below the set measurement limit of the sedigraph. Clay (here defined as < 2 μm) is the dominant size fraction with cumulative percentages ranging about 50% to 70%.

4.2.4. Description of the defined units

4.2.4.1. Unit 1: 3195–3095 cm (11.9–10.3 kyr). The PSD surface plot shows a broad modal ridge centred at ca. 2–4 μm at the bottom of the unit, moving towards a finer size at its younger end (Figs. 2 and 5). The PSD surface plot also shows a high degree of noise in unit 1, covering all sizes from the coarse end of the spectrum (63 μm) down to 22 μm in the old end, and broadening to cover the entire sortable silt interval (10–63 μm) in the younger parts of the unit (Figs. 2 and 5). The sortable silt median is highly variable, although a weak decreasing trend from ca. 15 μm to ca. 13 μm is discernible (Fig. 5). The median grain size is below 1 μm (Fig. 5), reflecting a high clay content. The coarse fraction (> 63 μm) in the beginning of unit 1 shows the highest values in the record (except for a few scattered samples in units 4 and 5), about 0.5%, followed by a distinct decreasing trend from ca. 11.9 kyr ending abruptly at 10.2 kyr (Fig. 5). Visual inspection of the coarse fraction shows that the > 63 μm material in unit 1 consists of either large (ca. 0.5–1.6 mm) grains of quartz, feldspar and dark crystalline and metamorphic rock fragments, or small (ca. 0.2 mm) grains of detrital carbonate and quartz (Fig. 6). With the addition of small amounts of foraminifera, shell fragments and pyrite, the latter composition generally occurs in all samples younger than ca. 10.2 kyr. The sortable silt content in unit 1 and the oldest part of unit 2 is close to 5% (Fig. 5), which is the lower limit for reliable interpretation of sedigraph data (Bianchi et al., 1999). The fine silt content in unit 1 is relatively low (Fig. 5) and generally mirrors the clay content. The clay content in unit 1 is markedly high, showing an increasing trend from 67% to 73% that begins at 11.3 kyr and ends abruptly by the end of the unit at 10.3 kyr (Fig. 5).

4.2.4.2. Unit 2: 3095–2747 cm (10.3–8.5 kyr). In the PSD surface plot, the modal ridge appears more pronounced, broader and more coarse-skewed in unit 2 than in unit 1 (Figs. 2 and 5). The noise-affected size interval in the PSD surface plot shows a slight decrease from unit 1 (Figs. 2 and 5). The sortable silt median variations have the highest amplitude in unit 2 (Fig. 5). The median grain size varies from below 1 μm to about 1.1–1.2 μm (Fig. 5). The coarse fraction in unit 2 shows variable values around 0.1% (Fig. 5), and visual inspection of the grains yields that only one sample from 3080 cm core depth (10.23 kyr) shows a composition similar to the samples from unit 1 (crystalline or metamorphic rock fragments and largest grains > 1 mm). All other coarse fraction samples from unit 2 consists of small (< 0.5 mm) grains of quartz and detrital carbonate and larger carbonate shell fragments. The sortable silt content in unit 2 is still very low, but shows an increasing trend from 5% to 6% (Fig. 5). The fine silt (Fig. 5) continues to mirror the clay content and shows a marked increase from 10.3 to ca. 9.4 kyr and a shift to higher values at 8.5 kyr. The clay content shows a marked decreasing trend through unit 2 and the decrease is most pronounced from 10.3 to 9.8 kyr (Fig. 5).

Fig. 5. Low-pass filtered version of the PSD surface plot (cf. Fig. 2) grain size parameters and carbonate content in core MD99-2286. Dotted vertical lines show the location of defined lithological unit boundaries, and the definition points are marked with arrows and roman numerals I–IV. The white dotted line in the PSD surface plot marks the grain size mode (visually estimated in Fig. 2). The black bars in the coarse fraction plot mark IRD based on visual inspection (see Fig. 6).

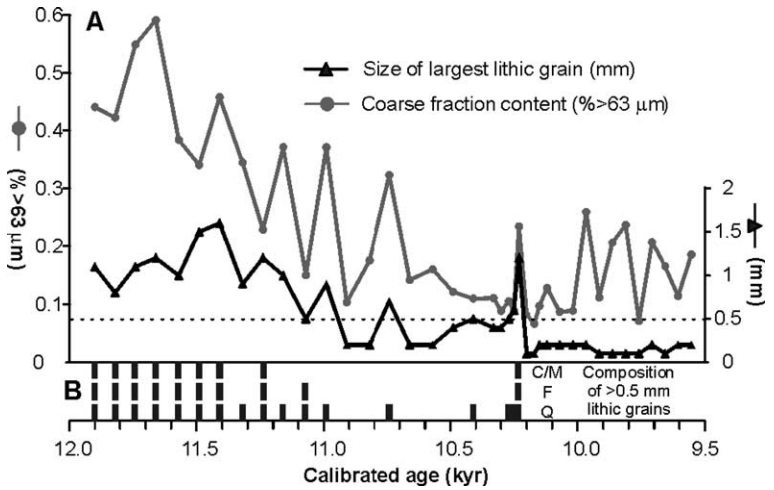

Fig. 6. Indications of IRD in core MD99-2286. (A) Coarse fraction content (grey curve) and size of the largest lithic grain in each sample (black curve). The dotted horizontal line marks the 0.5 mm limit. (B) Black bars below the corresponding samples from the curves above show the composition of lithic grains ≥ 0.5 mm, where Q=quartz, F=feldspar and C/M=crystalline/metamorphic rocks.

4.2.4.3. Unit 3: 2747–1765 cm (8.5–4.0 kyr). The PSD surface plot shows that the modal ridge shifts to 3 to 4 μm at the unit 2/3 boundary and becomes more pronounced in the older end of unit 3 (Figs. 2 and 5). The modal ridge is most pronounced in the entire record between 8.5 and 7.3 kyr. After 7.3 kyr, the modal ridge decreases and becomes more symmetrical (showing decreasing skewness) with time throughout the unit. The noise levels decrease abruptly at ca. 6.0 kyr, so that the finest size affected by noise change from 20 to 40 μm (Fig. 2). The sortable silt median is relatively stable at ca. 14 μm until ca. 7.0 kyr, and an increasing trend from 14 to 16 μm can be distinguished between 7.0 and 4.5 kyr (Fig. 5). The median grain size varies between 1.2 and 1.3 μm (Fig. 5). The coarse fraction in unit 3 shows little change from unit 2, although a small increasing trend starting at ca. 7.0 kyr can be distinguished (Fig. 5). The sortable silt percentage increases in a linear trend throughout the unit (Fig. 5). The fine silt shows a decreasing trend through unit 3, where the most rapid decrease occurs between 6.0 and 5.0 kyr (Fig. 5). The clay content shows a slightly decreasing trend through unit 3 (Fig. 5).

4.2.4.4. Unit 4: 1765–571 cm (4.0–0.9 kyr). The PSD surface plot shows that the modality continues to decrease and the modal ridge begins a weak trend from symmetrical to more fine skewed with decreasing age (Figs. 2 and 5). Noise levels in the sortable silt interval continue to decrease (Figs. 2 and 5). The sortable silt median is relatively stable around 15 μm, although a small increase between 1.5 and 0.9 kyr is discernible (Fig. 5). The median grain size shows a rapid increase until ca. 3.0 kyr, followed by a weak increasing trend through the rest of the unit (Fig. 5). The coarse fraction content and its amplitude are stable until 2.4 kyr, but displays an increasing trend from 2.4 kyr until the younger end of unit 4 (Fig. 5). The sortable silt continues the increasing trend from unit 3, with an increase in variability towards the younger end of the unit (Fig. 5). The fine silt content is relatively stable until 2.4 kyr, when a decreasing trend through the rest of the unit begins (Fig. 5f). The clay content decreases slightly between 4.0 and 3.0 kyr, and is relatively stable throughout the rest of unit 4 (Fig. 5).

4.2.4.5. Unit 5: 571–0 cm (0.9 kyr–recent). The PSD surface plot shows further decreased modality and increasing fine skewness throughout unit 5 (Figs. 2 and 5). The sortable silt median shows high and variable values through the unit (Fig. 5). The median grain size is marked by a remarkable peak in the beginning of unit 5 between ca. 0.6 and 0.9 kyr, and high and variable values in the younger parts of the unit (Fig. 5). The coarse fraction shows high and variable values throughout unit 5 (Fig. 5). The sortable silt content shows values among the highest

in the record between ca. 0.6 and 0.9 kyr, after which a weak decreasing trend through the unit is visible (Fig. 5), distinct from the increase observed through units 2, 3 and 4. The fine silt also shows high values between ca. 0.6 and 0.9 kyr, but is otherwise low and variable through unit 5 (Fig. 5). The clay content shows a pronounced low between ca. 0.6 and 0.9 kyr, and a weak decreasing trend through the younger parts of unit 5 (Fig. 5).

5. Discussion

5.1. MAR

Because of the linearly increasing density, the MAR curve for core MD99-2286 is driven by the age model's linear sedimentation rate. The actual sedimentation rate is a complex function of sediment supply and preservation. Major changes in the sedimentation rate are likely to be linked to changes in some lithological parameter such as grain size, composition or structure. Here grain size is used to guide selection of different unit boundaries used to describe the sediments in this core.

The lithological unit boundaries (Figs. 2 and 5) are defined where prominent changes in the grain size occur. Major changes in MAR (letters in Fig. 4) appear close to two of these boundaries. Assuming that the changes in MAR are associated with these changes in grain size, the timing of major MAR changes a and c (Fig. 4) are suggested to coincide with the unit boundaries at 10.3 and 4.0 kyr, respectively.

The MAR increase marked d in Fig. 4 is an exception, as no major grain size change occurs between the age control-points (2.0–1.4 kyr) for this shift. An increase in median grain size, coarse fraction content and sortable silt median size in unit 5 suggests ca. 0.3 kyr for the MAR increase marked V in Fig. 4, although the grain size change was not considered large enough to invoke a lithological boundary.

5.2. Carbonate

The correlation between carbonate and fine silt shows that a large proportion of the carbonate deposited in northeastern Skagerrak occurs in the fine silt (2–10 μm) fraction. Since this size fraction is largely cohesive (McCave et al., 1995), the carbonate particles were likely integrated in flocculated mud, and transported to the deposition area in suspension together with siliciclastic clay and fine silt.

The observed negative correlation between clay content and carbonate content in the core depth interval 3150–3070 cm, equivalent to 11.16–10.17 kyr, occurs in the interval with a pronounced increase in clay content. At the stepwise increase in MAR, induced by the apparent increase in linear sedimentation rate, the clay MAR shows a higher increase than the carbonate MAR (Fig. 4). Directly after the stepwise increase, the carbonate MAR increases gradually, whereas the clay MAR decreases. The clay and carbonate MARs (Fig. 4) thus show that the carbonate content was controlled by the diluting effect of increased clay deposition during this interval. This is interpreted as the result of mixing of different sediment sources during this time interval. Carbonate and siliciclastic material from a combination of sediment re-deposition, primary production and river input was probably transported to the MD99-2286 coring site from westerly sources such as the Atlantic Current and southern North Sea, whereas relatively fresh water with mostly clay sized siliciclastic sediments were brought to the site from continental Scandinavia in the east.

5.3. Grain size

Modelling of the floc-grain-settling process have illustrated how the grain size spectra changes with variations in transport energy, flocculation state, settling increment and number of resuspension events (Kranck, 1975, 1987; Kranck and Milligan, 1985, 1991). These general relationships form the basis of the interpretation of the PSD surface plots of the grain size record from core MD99-2286. The frequency spectra show a high proportion of fine material, which can be seen as a major hump in sizes smaller than 10 μm in the frequency plots and the PSD surface plot (Fig. 2). This relatively flat, non-modal or polymodal shape of the frequency curve in the fine end of the grain size spectrum is indicative of a high flocculation state (Kranck and Milligan, 1991; Kranck, 1975, 1987), where most of the sediment is carried as aggregates in suspension. A less prominent but persistent modal ridge in the coarse silt fraction can

be seen in large parts of the PSD, indicating that deposition of individual grains has occurred (Kranck and Milligan, 1991; Kranck, 1975, 1987). The coarse silt modal ridge is discernible both in the noise-free and in the noise-affected parts of the core. In the latter case, the coarse silt mode resembles a small ridge with grain size frequencies of up to ca. 0.6% in the 30–40 μm interval between blanked noise-troughs (white in Fig. 2). This is due to the occurrence of apparently sufficient amounts of material for adequate sedigraph readings in a part of the coarse silt fraction (the coarse silt ridge), surrounded by readings of coarser and finer sizes where the frequency of material was too low to accurately register.

5.3.1. Reconstructions of the paleo-sedimentary environment

5.3.1.1. 11.900–10.3 kyr (unit 1). The composition of the coarse fraction and the fact that the coarse grained material occurs in an otherwise fine grained matrix implies that the observed trend in the coarse fraction below 3080 cm core depth (i.e. older than ca. 10.2 kyr) is the result of a decreasing amount of ice rafted debris (IRD) in younger sediments. As the coarse fraction and the finer fractions thus likely are indicators of partly different processes–glaciomarine and "normal" marine sedimentation–these parameters will partly be treated separately in the following discussion.

5.3.1.2. IRD. The Oslofjord region was the last sea area of the Skagerrak region to be deglaciated, according to paleogeographic reconstructions (Stabell and Thiede, 1986; Thiede, 1987; Houmark-Nielsen and Kjaer, 2003; Lagerlund and Houmark-Nielsen, 1993) and dated end moraines onshore (Sørensen, 1992; Andersen et al., 1995; Lundqvist and Wohlfarth, 2001). Based on a compilation of dated ice grounding lines and the models presented by Boulton (1990), Sørensen (1992) concluded that there must have been a fairly high frequency of iceberg calving in the inner Oslofjord at the end of Younger Dryas. The MD99-2286 coring site is located in the northern flank of the Skagerrak southwest of the Oslofjord. Due to the cyclonic circulation, the main current flow passes the Oslofjord mouth on it way to the MD99-2286 coring site. This implies that during the final stages of the break-up of the shelf ice, icebergs passing over the MD99-2286 coring site probably originated from the Oslofjord. The occurrence of a 2-cm dropstone at 3164 cm core depth supports that ice rafting was still active at 11.5 kyr in the northeastern Skagerrak. The abrupt decrease of the coarse fraction content in core MD99-2286 implies that iceberg calving in the northeastern Skagerrak ceased at about 10.2 kyr.

Relatively little has been published about IRD in the early Holocene in the Skagerrak, and the timing when iceberg calving into the Skagerrak ended is unclear. Based on acoustic profiles and piston cores, van Weering (1982b) concluded that ice rafting ceased in southwestern Skagerrak before ca. 11.6–11.3 kyr (Table 1, event b). The grain size record of core GIK 15530-4 from 57.667°N, 7.092°E in the western Skagerrak indicated that IRD decreased to low values in the early Preboreal (Stabell et al., 1985; Werner, 1985).

The youngest sample showing signs of IRD in core MD99-2286 occurs at 3080 cm core depth, corresponding to ca. 10.2 kyr. The largest grains are ca. 1.2 mm in diameter and consist of crystalline and metamorphic rock fragments, similar to those in samples older than 11.2 kyr (Figs. 5 and 7). Between ca. 10.7 and 10.2 kyr, the coarse fraction content is lower, and the largest grains in all samples are smaller and consist of calcite or quartz (Fig. 6). A period of about 500 years virtually lacking IRD thus begins at 10.7 kyr. A final, isolated IRD peak occurs in a single sample at ca. 10.2 kyr (Fig. 6).

The highest marine limit in Norway is mapped to ca. 220 m and dated to about 11.2–10.8 kyr (Table 1, event d) in the Oslo area north of the Oslofjord (Fig. 7) (Hafsten, 1983). The Aker Ice Marginal Zone (Aker IMZ, Fig. 7), located ca. 5 km north of the innermost Oslofjord, comprises ice marginal ridges both above and below the marine limit and is also dated to about 11.2–10.8 kyr (Table 1, event c) (Sørensen, 1979; Gjessing, 1980; Gjessing and Spjeldnaes, 1979; Andersen et al., 1995). This implies that the retreating ice was separated from the sea in the Oslofjord at the latest about 10.8 kyr, which thus constitutes the youngest age of possible iceberg calving into the Oslofjord. The IRD-peak at just before 10.7 kyr in core MD99-2286 (Figs. 5 and 7) is interpreted to represent the end of iceberg calving,

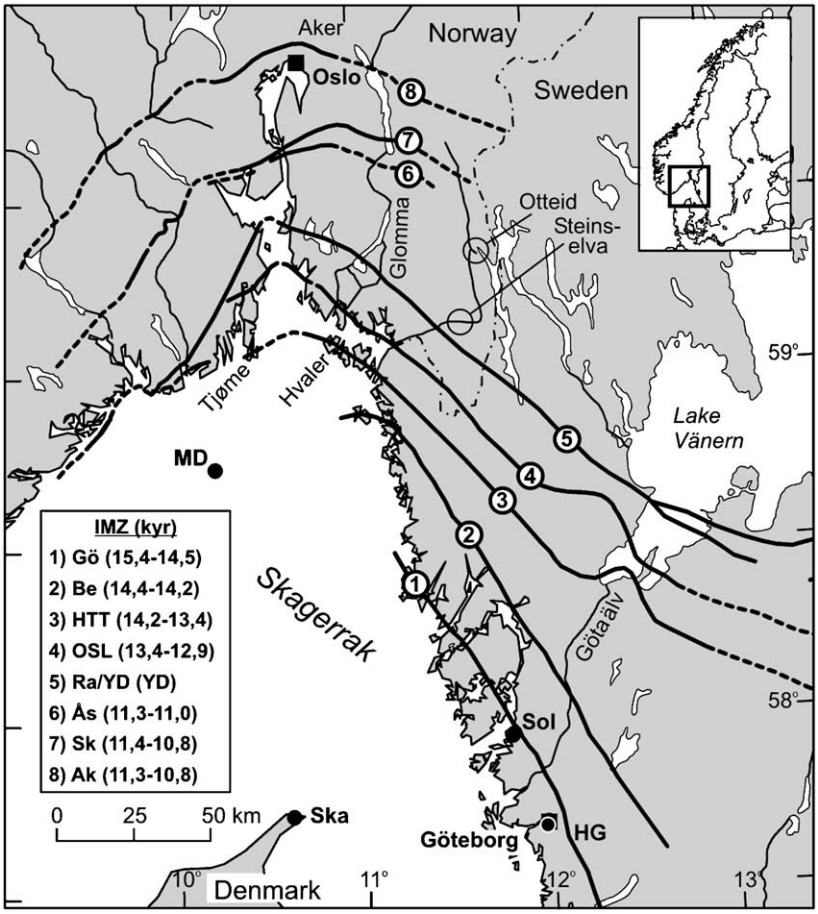

Fig. 7. Ice marginal zones (IMZ, numbers in circles) of the Oslo Fjord region and southwestern Sweden, compiled from Andersen et al. (1995), Sørensen (1992) and Lundqvist and Wohlfarth (2001). Solid lines indicate mapped IMZ positions and dashed lines mark inferred ice margins. (1) Gö=Göteborg Moraine, (2) Be=Berghem Moraine, (3) HTT=Hvaler/Tjøme-Trollhättan Moraines, (4) OSL=Onsøy/Slagen-Levene Moraines, (5) Ra/YD=Ra/YD Moraines, (6) Ås=Ås IMZ, (7) Sk=Ski IMZ, (8) Ak=Aker Moraine. Ages for IMZ 1, 2, 4 and 5 and the oldest IMZ 3 age are from Lundqvist and Wohlfarth (2001). The youngest IMZ 3 age located at Tjøme and ages for IMZ 6–8 were calibrated (this work) from ^{14}C ages of Andersen et al. (1995), and the youngest IMZ 4 age located at Onsøy was calibrated (Gyllencreutz et al., 2005) from a ^{14}C age of Sørensen (1992). Locations of mentioned cores are shown with black dots, where MD=MD99-2286, Ska=Skagen 3, Sol=Solberga-2 and HG=Horticultural Garden. OF marks the Oslo Fjord. Modified after Gyllencreutz et al. (2005).

after which no IRD signal occur for almost 500 years. It follows that the sample from ca. 10.2 kyr represents a discrete, sudden event of increased ice rafting after the ice had retreated onshore. A possible explanation for this could be that the youngest IRD signal was caused by flood-transported icebergs in connection with the sudden drainage of an ice-dammed lake in southern Norway (referred to as the Glomma event below), which was described by Longva and Bakkejord (1990) and Longva and Thoresen (1991). The Glomma event was dated using terrestrial macrofossils to 10.4–10.2 kyr (Table 1, event e) (Oddvar Longva, pers. comm., 2004-06-04). The Glomma event emptied nearly 100 km^3 of water through four outlets, of which three emerge in the Oslofjord and one in the Vänern basin, causing severe erosion of the soft sediments. The erosion was caused by a combination of current winnowing and iceberg scouring, as indicated by abundant iceberg scours and iceberg gravity craters in the flooded area (Longva and Bakkejord, 1990; Longva and Thoresen, 1991). Icebergs that were not grounded during the

flooding likely emerged into the Skagerrak via the Oslofjord. It is therefore suggested that the youngest occurrence of IRD in the MD99-2286 record reflects iceberg transport caused by the catastrophic Glomma-event flooding, rather than by icebergs expelled directly into the sea from a calving ice front.

5.3.1.3. Clay content. The grain size record of core MD99-2286 does not show any distinct changes between 11.9 and 11.3 kyr, which implies that the final drainage of the Baltic Ice Lake (BIL) at ca. 11.6 kyr (Björck, 1995; Andrén et al., 2002; Björck et al., 2002) did not have a significant impact on the sedimentation in the northeastern Skagerrak.

The increasing clay content between 11.3 and 10.3 kyr is interpreted to reflect discharge from the Baltic Sea via the Vänern basin through outlets in south-eastern Norway and on the Swedish west coast in connection with the Yoldia Sea and the subsequent Ancylus Lake. The Otteid-Stenselva strait was the northernmost of the outlets across middle Sweden that opened a few hundred years after the final drainage of the BIL at ca. 11.6 kyr (Björck, 1995; Björck et al., 2002; Andrén et al., 2002). The Otteid-Stenselva functioned together with the Uddevalla Strait and the Göta Älv River as the major drainage routes from the Vänern basin (Fig. 8) during the Ancylus transgression (Björck, 1995). Due to a north–southerly difference in isostatic uplift, the narrow Otteid-Stenselva strait was closed at ca. 10.4–10.2 kyr (Table 1, event f), whereby the Göta Älv River became the dominant outlet (Björck, 1995; Lambeck, 1999). The age range of this closing correlates with the end of the clay increase in core MD99-2286 at 10.3 kyr.

Similar units with high clay contents are reported from several sites along the Swedish west coast, e.g. from sections, cores and seismic profiles in the Varberg area (Klingberg, 1996), from the Horticultural Garden core in Gothenburg (Fig. 8) (Bergsten, 1989, 1991, 1994) and from the Solberga-2 core (Fig. 8) (Cato et al., 1982). Bergsten (1994) interpreted that these deposits, referred to as unit B, reflect the

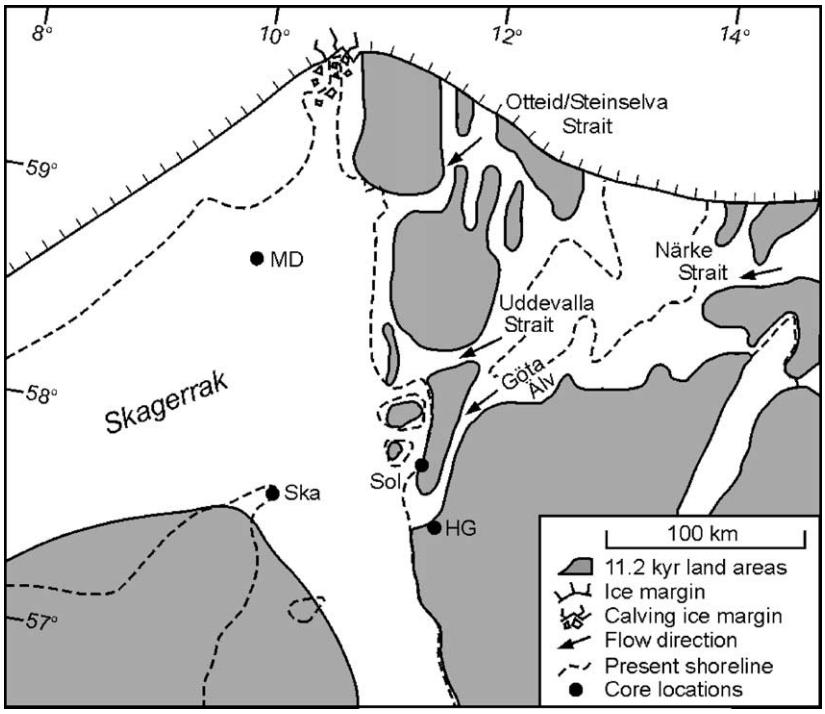

Fig. 8. Position of the Scandinavian Ice Sheet and paleo-shorelines in the Oslo Fjord region at 11.2 kyr, 100–200 years after the Närke Strait opened. Major outlets are named and shown with arrows indicating flow direction. Black dots mark the location of cores, where MD=MD99-2286, Ska=Skagen 3/4, Sol=Solberga-2 and HG=Horticultural Garden. Modified after Björck (1995).

discharge of meltwater in connection with the damming of the Ancylus Lake, based on the increased clay content and fresh water-influenced foraminiferal assemblages in the Horticultural Garden core. Bergsten (1994) further argued that unit B deposits, with characteristically high clay content, low cation content and fresh-water influence of foraminifers and diatoms, could be used as a regional stratigraphic marker unit. The Solberga-2 core was subsequently AMS ^{14}C dated by Bodén et al. (1997).

5.3.1.4. Dating and correlation of 'unit B'-type deposits in previous cores. Unit B (5.4 to 8 m core depth) of Bergsten (1994) was deposited between ca. 10.2 and 9.1 kyr, based on the 1993 calibration data set (Stuiver and Braziunas, 1993), which differs slightly from the MARINE98 calibration data set (Stuiver et al., 1998b) used for core MD99-2286 (Gyllencreutz et al., 2005). The age difference for the discussed interval is small and therefore considered negligible.

The chronostratigraphy of core Solberga-2 is more complicated. In the chronostratigraphy of core Solberga-2 proposed by Bodén et al. (1997), the two dated samples above 1330 cm core depth were discarded from the age model due to supposed reworking (Table 3, Fig. 9). However, there are no signs of major core disturbances in the X-ray images, photographs or core descriptions from core Solberga-2 (Abrahamsen, 1982). The age model of Bodén et al. (1997) infers a sedimentation rate lowered by a factor of > 6 above 18 m core depth relative to deeper parts of the core. This contradicts the interpretation of the Solberga-2 record, where variations in paleomagnetic records together with grain size data and fossil contents indicate increased sedimentation rate by a factor of 2–3 in the 17–12 m core depth interval relative to the deeper parts (Abrahamsen, 1982). An alternative age model is presented in Fig. 10, based on calibration of the Bodén et al. (1997) age estimates. The revised age model is constructed to be consistent with the paleomagnetic, sedimentological and faunal interpretations of the Solberga-2 core, thus omitting the two youngest of the Bodén et al. (1997) age control points (Table 3).

The younger age boundary of the clay unit at 6.7 m in core Solberga-2 cannot be determined because of lacking chronostratigraphic control. The onset of the clay content increase at 17.7 m core depth in Solberga-2 is dated to ca. 10.7 kyr based on the age model of Bodén et al. (1997) and ca. 11.1 kyr based on the alternative age model proposed here (Fig. 9). Regardless of which age model is used, a pattern of a successive shift towards the south of unit B type sediment deposition is evident. The increase in clay content in cores from north to south starts at ca. 11.3 kyr in core MD99-2286 (58.74°N), between ca. 11.1 and 10.7 kyr in core Solberga-2 (57.95°N), and at ca. 10.2 kyr in the Horticultural Garden core (57.70°N). Thus, a successive southward shift is evident of the depositional area for sediments originating from Baltic Sea outflow, coherent with a north–south differential uplift (Lambeck, 1999). This scenario supports the course of events proposed by Bergsten

Table 3
Calibration of AMS ^{14}C dates from core Solberga-2

Laboratory reference	Depth	^{14}C age ± 1σ	Age range (cal. years BP) probability method		
	(m)	(y BP)	Max (1σ)	Median	Min (1σ)
OS-4532[a]	11.25–11.40	9610 ± 45	10,344	10,316	10,194
Uu-10300[a,b]	11.40–11.55	8885 ± 90	9624	9429	9361
Uu-10301[b]	13.30–13.55	4550 ± 80	4832	4733	4633
OS-4527[b]	15.30–15.55	7730 ± 85	8298	8185	8103
OS-4528	18.15–18.30	10,300 ± 110	11,375	11,244	11,114
OS-4526[a,b]	19.30–19.35	10,800 ± 85	12,347	12,131	11,918
OS-4529	22.00–22.30	10,700 ± 75	12,146	11,926	11,665
OS-4530	26.50–26.60	11,600 ± 95	13,183	13,098	12,917
OS-4531	27.30–27.35	12,400 ± 95	14,094	13,940	13,802

[a] Samples omitted from the Solberga-2 age model by Bodén et al. (1997).
[b] Samples omitted from the new proposed Solberga-2 age model.

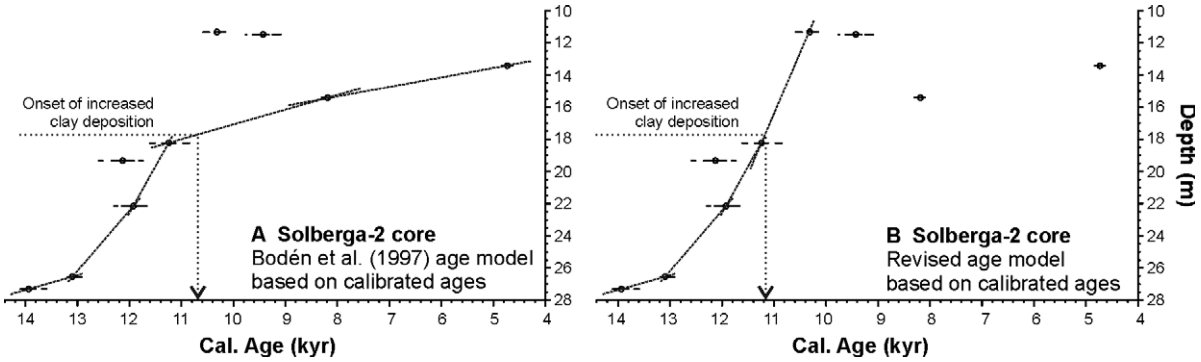

Fig. 9. Alternative age models for core Solberga-2 based on calibrated ages. (A) Calibrated age model using the same dates as Bodén et al. (1997). (B) Revised age model, based on the dates that give the best consistency with previous paleoenvironmental interpretations of the core. The calibrated median ages are shown with circles and 1σ ranges are marked with black lines through the dates. The horizontal dotted line marks the stratigraphical level for the onset of increased clay content at 17.7 m (Cato et al., 1982). The inferred calibrated age estimates for the 17.7 m level are marked with vertical dot-dashed lines in both age models.

(1994) and Björck (1995) despite the uncertainty in the Solberga-2 chronology.

The time interval of 500 to 900 years between the onset of increased clay deposition at the Solberga-2 and the Horticultural Garden sites is relatively long despite the short distance between them. This may be explained by the fact that these sites were separated by a NNE–SSW trending ridge west of the Göta Älv river valley (Fig. 8), allowing water to reach the Solberga-2 site from outflow through the northerly

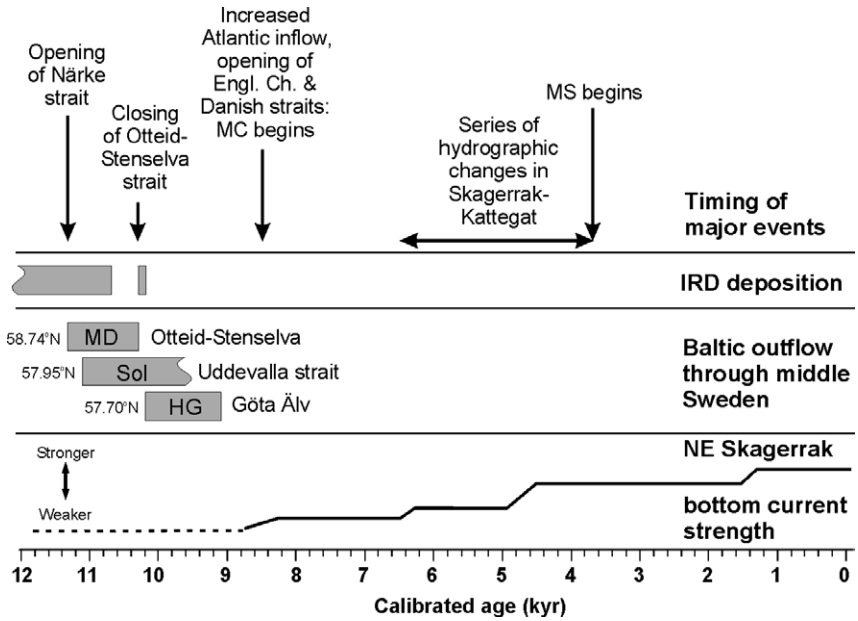

Fig. 10. Schematic compilation of important circulation and sedimentation features in the Skagerrak during the late Glacial and the Holocene. "MC begins" refers to the initiation of the modern type of circulation in the Skagerrak–Kattegat. "MS begins" refers to the development of the modern type of sedimentation pattern in the Skagerrak–Kattegat. MD, Sol and HG indicate results from the cores MD99-2286, Solberga-2 and Horticultural Garden, respectively. The interpreted bottom current strength is based on the sortable silt median (Fig. 5) and the dashed line indicates an interval where this proxy is less reliable due to low amounts of sortable silt (Fig. 5).

Uddevalla Strait (Fig. 8), whereas the Horticultural Garden site received its input from the Göta Älv River (Björck, 1995).

5.3.1.5. Unit 2. The distinct decreasing trend in clay content between 10.3 and 9.5 kyr is not correlated to changes in the PSD surface plot, sortable silt or coarse fraction (Figs. 2 and 5), suggesting that the cause is related to changes in sediment source and composition rather than in the sedimentation process. The end of the increase in clay content at ca. 10.3 kyr coincides with the closing of the Otteid-Stenselva outlet when the threshold was uplifted above sea level (Björck, 1995; Lambeck, 1999). Because of this, the main route of the Baltic Sea outflow was directed further south and caused increased clay contents in the Solberga-2 site and eventually the Horticultural Garden site. When the Baltic Sea outflow through the Otteid-Stenselva ceased, the ice sheet had recessed far inland (Fig. 7) and glacial meltwater no longer had a large impact in the Skagerrak (Jiang et al., 1997). The decreasing clay content in core MD99-2286 is therefore interpreted as a consequence of decreasing influence of sediments from glacial meltwater, when the Skagerrak started to gradually adapt to a full-interglacial marine sedimentation mostly influenced by Atlantic water and the North Jutland Current. This is supported by indications of stronger Atlantic water inflow in the beginning of the Holocene from the Norwegian Channel (Klitgaard-Kristensen et al., 2001) and the Skagerrak (Jiang et al., 1997; Conradsen and Heier-Nielsen, 1995).

The abrupt modal shift towards coarser grain size, from 3 to 4 μm at the end of unit 2 at ca. 8.5 kyr (Figs. 2 and 5), indicates an increase in transport energy (Kranck, 1987, 1975; Kranck and Milligan, 1991, 1985). This shift is also manifested as an abrupt decrease in the variance of the sortable silt median, an increase in median grain size, an increase in fine silt and a decrease in clay content (Fig. 5). The high variance in the sortable silt median in unit 2 cannot be entirely explained by the low amounts of material, because the variance decreases abruptly at 8.5 kyr, whereas the sortable silt content increases gradually until the young end of unit 4. Because of the low amounts of material in the sortable silt fraction, a few anomalously large silt grains would have a large effect on the sortable silt median size in unit 2. The high variance in the sortable silt median size in unit 2 is therefore interpreted to reflect a weak bottom current with a variable concentration of sortable silt. The sudden decrease in amplitude of the sortable silt median, the increase in median size, decrease in clay content and the modal shift towards coarser grain size indicates a hydrographic shift at 8.5 kyr.

The hydrographic shift recorded in core MD99-2286 at 8.5 kyr may be correlated to changes reported in several studies from the Norwegian Channel and the Skagerrak–Kattegat, if allowing for some variability in the age estimates (Klitgaard-Kristensen et al., 2001 (9.0 kyr); Conradsen and Heier-Nielsen, 1995 (8.5 kyr, Table 1, event h); Conradsen, 1995 (9.0–8.7 kyr, Table 1, event m); Jiang et al., 1997 (8.6 kyr, Table 1, event i); Nordberg, 1991 (9.0–8.7 kyr, Table 1, event g); Björklund et al., 1985 (9.0–7.7 kyr, Table 1, event j)). All studies suggest that the opening of the English Channel and subsequent formation of the South Jutland Current, marking the establishment of the modern surface current system in the Skagerrak, occurred 9.0–8.0 kyr.

The Jutland Current today consists of two branches, the South Trench Current and the South Jutland Current (Nordberg, 1991). The former flows along the southern flank of the Norwegian Trench and supplies large volumes of Atlantic Water to the Skagerrak, accounting for about 90% of the inflow (Longva and Thorsnes, 1997). The latter flows northward near Danish coast over sand-dominated sediments (Longva and Thorsnes, 1997) and is the most erosive of the branches, transporting the highest concentrations of suspended sediment (Eisma and Kalf, 1987). The South Jutland Current is a low-volume water body and delivers less sediment to the Skagerrak than the South Trench Current, despite the high sediment concentrations. The markedly low amounts of sortable silt in units 1 and 2 of core MD99-2286 support the interpretation that the South Jutland Current was virtually absent before 8.5 kyr.

In the Norwegian Channel, a pronounced warming in the surface and bottom water masses associated with a strengthening of the Atlantic water inflow occurred at ca. 9.0 kyr based on foraminiferal assemblages and stable isotope data in cores 28-03, Troll 89-03 and Troll 91-1 (Klitgaard-Kristensen et al., 2001). They correlated this change to the hydrographic shift recorded in the Skagen 3/4 core at 8.6–

8.5 kyr (Table 1, events h–i) (Jiang et al., 1997; Conradsen and Heier-Nielsen, 1995). The increase in Atlantic water influence was recorded in core GIK 15530-4 from the western Skagerrak at ca. 9.0–7.7 kyr (Table 1, event j) (Björklund et al., 1985). A change in environmental and sedimentological conditions has been recorded in the Kattegat at 9.0–8.7 kyr (Table 1, events g and m) (Conradsen, 1995; Nordberg, 1991). This change was interpreted by Conradsen (1995) to reflect the opening of a connection to the Baltic Sea via the Danish straits at 9.0–8.7 kyr (Table 1, event l) (Lambeck, 1999). The hydrography of the southern Kattegat may have been more influenced than the Skagerrak by the opening of a connection to the Baltic (Conradsen, 1995).

Isostatic rebound modelling suggests that the English Channel opened at ca. 9.0–7.7 kyr (Table 1, event k) (Lambeck, 1995). Other important factors for the circulation in the early Holocene Skagerrak include the isolation of the Dogger Bank as an emerged platform and the transgression over large former land areas south–west of the present Danish coast shortly after ca. 9.0 kyr (Table 1, event o) (Lambeck, 1995; Jelgersma, 1979). This permitted Atlantic water from the southwestern North Sea to flow counter-clockwise around the Dogger Bank towards Denmark, possibly initiating a relatively weak South Jutland Current flow.

To conclude, major hydrographic shifts occurred in the Norwegian Channel and the Skagerrak–Kattegat around 8.5 kyr, attributed to increased Atlantic water inflow and transgression of the southern North Sea and to the opening of the English Channel and the Danish straits. All of these changes were necessary prerequisites for the establishment of the modern general circulation. The consistent results from the Skagerrak cores suggest that a circulation pattern similar to the present has persisted since 8.6–8.5 kyr.

5.3.1.6. Unit 3. After the abrupt shift at 8.5 kyr, the modal ridge begins a trend towards decreasing modal strength throughout the core (Figs. 2 and 5). The decrease in modal strength is most pronounced from 7.0 kyr throughout unit 3 and is interpreted as the result of an increased proportion of floc-settled material (Kranck and Milligan, 1991). At about 7.0 kyr, the sortable silt median starts a trend towards coarser values throughout unit 3 (Fig. 5). Such a trend typically indicates increasing transport energy (McCave et al., 1995). During this time, the modal ridge migrates towards coarser grain sizes (Figs. 2 and 5), which is a further indication of increased transport energy (Kranck and Milligan, 1991). Flocculation is primarily controlled by the concentration of particulate matter (Kranck, 1981) and is promoted by moderate turbulence (van Leussen, 1994), which in turn is promoted by higher velocity. The observed coarsening in the sortable silt median and the coarse-migration of the modal ridge are thus coherent with the interpreted increase in flocculation and are interpreted as a result of a gradually stronger current system with an increasing concentration of sediment. This is consistent with the paleoceanographic interpretations from diatoms in the Skagen 3/4 core (Jiang et al., 1997), where a strengthening of the South Jutland Current and increased influence of the Norwegian Coastal Current and the currents along the Swedish west coast occurred between 8.6 and 5.9 kyr (Table 1, events i and q).

5.3.1.7. Unit 4. The median grain size increases markedly between ca. 4.5 and 3.8 kyr. This increase reflects an overall coarsening of the sediment, which can also be seen as a decrease in clay content and a small increase in sortable silt and coarse fraction.

A large hydrographic change at 4.6–4.3 kyr (Table 1, event r) was suggested by Nordberg and Bergsten (1988) and Nordberg (1991), based on changes in sedimentology and in foraminifer assemblages, in several cores from the Skagerrak and the Kattegat. Nordberg (1991) proposed that this shift marks the establishment of the modern surface current pattern. This change has been correlated to a hydrographic shift at ca. 6.2–5.9 kyr (Table 1, events p–q) based on a distinct change in lithology, foraminifers and diatoms in the Skagen 3/4 core by Jiang et al. (1997) and Conradsen and Heier-Nielsen (1995), and based on foraminifer assemblages in piston cores from the Kattegat (Conradsen, 1995). These authors proposed a shift to higher energy conditions and an acceleration of the Jutland Current in connection with climatic cooling, and argued that the alleged changes at 6.2 and 4.6–4.3 kyr (Table 1, events p and r) represent a single event at 6.2 kyr (Table 1, event p). Core MD99-2286 shows a fluctuation and a small coarsening in the modal ridge of the PSD surface plot

around 6.3 kyr (Figs. 2 and 5), along with minor changes to increased sortable silt median size, median grain size and coarse fraction (Fig. 5). The change at 6.3 kyr in core MD99-2286 can thus be viewed as the first of a series of changes ending at ca. 3.8 kyr.

The main controlling factor of the Skagerrak–Kattegat circulation system is the inflow of Atlantic Water (Longva and Thorsnes, 1997; Svansson, 1975). The Skagen 3/4 core (Conradsen and Heier-Nielsen, 1995) is located in a position more susceptible to changes in the strength the South Jutland Current, and thus the transport and deposition of erosional products from the Danish west coast (Longva and Thorsnes, 1997), than the MD99-2286 site and the Kattegat sites. Conversely, the coring locations of Conradsen (1995), Nordberg (1991) and Nordberg and Bergsten (1988) from the Kattegat and southeastern Skagerrak are more susceptible to local variations in the mixing of the North Jutland Current and Baltic Sea outflow (Longva and Thorsnes, 1997; Conradsen, 1995; Nordberg and Bergsten, 1988) than the northerly Skagerrak sites. The coring location of core MD99-2286 is less biased towards the Jutland Current or the Baltic Sea outflow. It is therefore suggested that the hydrographic shifts recorded in the interval 6.2–3.8 kyr in core MD99-2286 and in other sites in the Skagerrak–Kattegat (Jiang et al., 1997; Conradsen and Heier-Nielsen, 1995; Conradsen, 1995; Nordberg, 1991; Nordberg and Bergsten, 1988) belong to a continuous hydrographic transition spanning ca. 2000 years. The sedimentary changes during this long interval are differently manifested in different parts of the Skagerrak–Kattegat region, depending on its complex circulation system.

The sortable silt median increases at 1.3 kyr, after which it is relatively stable until present times. This suggests that the modern current strength at the MD99-2286 site was attained at about 1.3 kyr, which is in agreement with conclusions by Hass (1996).

5.3.1.8. Unit 5. The remarkable change in core MD99-2286 around the unit 4/5 boundary marks the onset of an event from 0.9 to 0.6 kyr, showing a distinct coarsening of the sediments (Figs. 2 and 5). The sortable silt median remains largely unaffected (Fig. 5), which implies that the change in grain size distribution is not related to current speed at the deposition site (McCave et al., 1995). The negative correlation in this interval between clay (which is the main constituent with > 50%; Fig. 5) and the fine-and sortable silt fractions (ca. 28% and 22%, respectively; Fig. 5) could be a spurious effect of data closure, i.e. a result of grain sizes given as percentages. The low clay content and increased coarse fraction indicates increased deposition from the bottom nepheloid layer. This could be caused by increased current strength and erosion along the shallow, sand-dominated (Longva and Thorsnes, 1997) Danish west coast leading to higher concentrations of coarse material, subsequently deposited in the deeper, relatively quiet waters in the northeastern Skagerrak.

Grain size analysis of late Holocene sediments has been previously studied in four cores from the southern flank of the Skagerrak by Hass (1996), where grain size variations in the cores were correlated to climate fluctuations. Hass (1996) noticed that warmer climate periods are characterized by finer sediments due to weaker bottom currents, possibly resulting from a more northerly location of cyclone tracks making the Skagerrak less frequently affected by strong westerly winds. Hass (1996) also suggested that colder climate periods are generally characterized by coarser sediments due to higher current energies and by higher sedimentation rates in the eastern Skagerrak, as consequences of frequent current pulses due to a southward movement of the main zone of strong westerly winds and cyclones.

The event around 0.9 kyr in core MD99-2286 may be correlated to a peak with about 100–200 years duration in the 63–125 μm grain size fraction ("FSD 3a", Hass, 1996) in the cores II KAL, III KAL and 15535-1, retrieved from the southern flank of the Skagerrak at 245, 450 and 428 m water depth, respectively. This peak was interpreted as the result of a short-term cold spell with increased winter storminess, in an otherwise warm climate phase with little storm activity (Hass, 1996).

The grain size record indicates a small shift in the sedimentation at ca. 0.8 kyr, as the sortable silt content for the first time starts a decreasing trend, lasting into the present. The sortable silt median shows high and variable but stationary values and the coarse fraction shows a trend towards higher and more variable values during the same interval. The high variability during the last 800 years through present days

indicates a current system significantly modified by regional climatic conditions.

It is possible that the grain size distribution in the northeastern Skagerrak has been affected by anthropogenic influence such as deforestation and river regulation during the late Holocene. However, the major rivers of Norway and Sweden discharge into fjords, where most of the sediment load is trapped within the fjord sills, resulting in a relative minor sediment contribution from rivers to the Skagerrak (Longva and Thorsnes, 1997). The strongly variable grain size fluctuations during the last 2000 years are therefore not likely caused by human changes to the hydrographic environment.

The present situation represents the continuation of a general trend of coarsening, poorer sorting and increasing variability in core MD99-2286 since the modern circulation system began to be developed at ca. 8.5 kyr. This trend is mainly attributed to increasing sediment transport and strength of the South Jutland Current, which is largely dependent on the regional wind stress over the southern North Sea (Rodhe, 1996), and of the Atlantic water inflow (Longva and Thorsnes, 1997). In this perspective, the grain size record of core MD99-2286 shows an increasing dependence of the regional climate through most of the Holocene.

6. Conclusions

A schematic compilation of the interpreted circulation and sedimentation features is presented in Fig. 10. Seven important features of the development of the circulation and sedimentation in the northeastern Skagerrak are inferred from the MD99-2286 grain size record and comparison with previous studies:

(1) Iceberg calving in the Skagerrak ended between 10.7 and 10.2 kyr.
(2) A distinct increase in clay content starting at ca. 11.3 kyr and abruptly ending at ca. 10.3 kyr is attributed to outflow from the Baltic through the Otteid-Stenselva strait in southeastern Norway in connection with the Yoldia Sea and the subsequent Ancylus transgression in the Baltic Sea basin. The timing of the end of the increase in clay content matches the closing of the Otteid-Stenselva passage.
(3) The increased clay content between 11.3 and 10.3 kyr is correlated to similar clay-rich units in cores and sections from the Swedish west coast. The onset of this clay-rich deposition occurs progressively later in cores further south along the coast, supporting a previously proposed hypothesis that differential glacio-isostatic uplift caused a southward migration of the main depositional area for the Baltic outflow sediments.
(4) A hydrographic shift to higher energy conditions in the Skagerrak occurred at 8.5 kyr and is manifested as a distinct coarsening of the sediments in core MD99-2286. This shift reflects the establishment of the modern circulation system in the eastern North Sea, which previously has been detected in the Skagerrak (Björklund et al., 1985; Jiang et al., 1997; Conradsen and Heier-Nielsen, 1995), the Kattegat (Conradsen, 1995; Nordberg, 1991; Nordberg and Bergsten, 1988) and in the Norwegian Channel (Klitgaard-Kristensen et al., 2001). The observed changes are attributed to the opening of the English Channel and the Danish straits, increased Atlantic water inflow and the development and increasing influence of the South Jutland Current.
(5) A series of changes from ca. 6.3 to ca. 3.8 kyr is considered to reflect strengthening of the Jutland Current and development towards the present day sedimentation system in the Skagerrak–Kattegat. These changes are correlated to previously reported hydrographic shifts at 6.2 kyr in the Skagerrak (Jiang et al., 1997; Conradsen and Heier-Nielsen, 1995) and 4.5 kyr in the Kattegat (Nordberg, 1991, Nordberg and Bergsten, 1988). It is suggested that these shifts were not synchronous, but separate features of a long transitional period related to strengthening of the current system. Owing to the complex circulation system, the resulting changes are differently manifested in different parts of the Skagerrak–Kattegat.
(6) The last 800 years are characterised by poorly sorted sediments with a relatively high, variable proportion of coarse material, reflecting a circu-

lation system significantly modified by regional climatic conditions, especially the general wind directions and storm frequency over the southern North Sea.

(7) A general trend of coarsening, poorer sorting and increasing variability in the MD99-2286 grain size record is discernible since ca. 8.5 kyr. This trend is mainly attributed to increasing strength and influence of the variable South Jutland Current, reflecting an increasing dependence of the regional climate.

Acknowledgements

The project supervisors Jan Backman and Eve Arnold are thanked for great support and encouragement through the study. The author is grateful to Thomas Andrén, Martin Jakobsson, Karen Luise Knudsen, Svante Björck, Risto Kumpulainen and Tom Flodén for fruitful discussions. Intergraph GeoMedia Professional facilitated the drawing of maps. This project was funded through grants to Jan Backman. Financial support from EU-HOLSMEER and the Swedish Research Council is greatly appreciated. The author is also grateful to Reidulv Bøe and an anonymous reviewer for constructive criticism.

References

Abrahamsen, N., 1982. Magnetostratigraphy. In: Olausson, E. (Ed.), The Pleistocene/Holocene Boundary in South-Western Sweden, Geological Survey of Sweden, vol. C794, pp. 93–119.

Andersen, B.G., Mangerud, J., Sørensen, R., Reite, A., Sveian, H., Thoresen, M., Bergström, B., 1995. Younger Dryas ice-marginal deposits in Norway. Quaternary International 28, 147–169.

Andrén, T., Lindeberg, G., Andrén, E., 2002. Evidence of the final drainage of the Baltic Ice Lake and the brackish phase of the Yoldia Sea in glacial varves from the Baltic Sea. Boreas 31, 226–238.

Bard, E., Hamelin, B., Fairbanks, R.G., Zindler, A., 1990. Calibration of the ^{14}C timescale over the past 30 000 years using mass spectrometric U–Th ages from Barbados corals. Nature 345, 405–410.

Beierle, B.D., Lamoureux, S.F., Cockburn, J.M.H., Spooner, I., 2002. A new method for visualizing sediment particle size distributions. Journal of Paleolimnology 27, 279–283.

Berglund, B.E., 1979. The deglaciation of southern Sweden 13 500–10 000 B.P.. Boreas 8, 89–118.

Bergsten, H., 1989. Stratigraphy of a late Weichselian–Holocene clay sequence at Göteborg, south-western Sweden. Department of Geology, Chalmers University of Technology and University of Gothenburg, A 68, 1–115.

Bergsten, H., 1991. Late Weichselian–Holocene stratigraphy and environmental conditions in the Gothenburg area, south-western Sweden. Department of Geology, Chalmers University of Technology and University of Gothenburg A 70, 1–109.

Bergsten, H., 1994. A high-resolution record of late Glacial and early Holocene marine sediments from southwestern Sweden; with special emphasis on environmental changes close to the Pleistocene–Holocene transition and the influence of fresh water from the Baltic basin. Journal of Quaternary Science 9, 1–12.

Bianchi, G.G., Hall, I.R., McCave, I.N., Joseph, L., 1999. Measurement of the sortable silt current speed proxy using the Sedigraph 5100 and Coulter Multisizer IIe: precision and accuracy. Sedimentology 46, 1001–1014.

Björck, S., 1995. A review of the history of the Baltic Sea, 13.0–8.0 ka BP. Quaternary International 27, 19–40.

Björck, J., Andrén, T., Wastegård, S., Possnert, G., Schoning, K., 2002. An event stratigraphy for the last Glacial–Holocene transition in eastern middle Sweden: results from investigations of varved clay and terrestrial sequences. Quaternary Science Reviews 21, 1489–1501.

Björklund, K.R., Bjørnstad, H., Dale, B., Erlenkeuser, H., Henningsmoen, K.E., Høeg, H.I., Johnsen, K., Manum, S.B., Mikkelsen, N., Nagy, J., Pederstad, K., Qvale, G., Rosenqvist, I.T., Salbu, B., Schoenharting, G., Stabell, B., Thiede, J., Throndsen, I., Wassman, P., Werner, F., 1985. Evolution of the upper Quaternary depositional environment in the Skagerrak: a synthesis. Norsk Geologisk Tidsskrift 65, 139–149.

Bodén, P., Fairbanks, R.G., Wright, J.D., Burckle, L.H., 1997. High-resolution stable isotope records from southwest Sweden: the drainage of the Baltic Ice Lake and Younger Dryas ice margin oscillations. Paleoceanography 12 (1), 39–49.

Bondevik, S., Birks, H.H., Gulliksen, S., Mangerud, J., 1999. Late Weichselian marine ^{14}C reservoir ages at the western coast of Norway. Quaternary Research 52, 104–114.

Boulton, G.S, 1990. Sedimentary and sea level changes during glacial cycles and their control on glaciomarine facies architecture. In: Dowdeswell, J.A., Scourse, J.D. (Eds.), Glacimarine Environments: Processes and Sediments, vol. 53. Geological Society Special Publication, vol. 53, pp. 15–52.

Bøe, R., Thorsnes, T. (Eds.), 1996. Marine Geology in the Skagerrak and Kattegat, Geological Survey of Norway Bulletin, vol. 430, pp. 1–144.

Bøe, R., Rise, L., Thorsnes, T.H., de Haas, H., Saether, O.M., Kunzendorf, H., 1996. Sea-bed sediments and sediment accumulation rates in the Norwegian part of Skagerrak. Geological Survey of Norway Bulletin 430, 75–84.

Cato, I., Fredén, C., Olausson, E., 1982. Summary of the investigation. In: Olausson, E. (Ed.), The Pleistocene/Holocene Boundary in South-Western Sweden. Geological Survey of Sweden, vol. C794, pp. 253–268.

Coakley, J.P., Syvitski, J.P.M., 1991. Sedigraph technique. In: Syvitski, J.P.M. (Ed.), Principles, Methods and Application of

Particle Size Analysis. Cambridge University Press, Cambridge, pp. 129–142.
Conradsen, K., 1995. Late Younger Dryas to Holocene palaeoenvironments of the southern Kattegat, Scandinavia. The Holocene 5 (4), 447–456.
Conradsen, K., Heier-Nielsen, S., 1995. Holocene paleoceanography and paleoenvironments of the Skagerrak–Kattegatt, Scandinavia. Paleoceanography 10, 810–813.
Danielssen, D.S., Edler, L., Fonselius, S., Hernroth, L., Ostrowski, M., Svendsen, E., Talsepp, L., 1997. Oceanographic variability in the Skagerrak and northern Kattegat, May–June 1990. ICES Journal of Marine Science 54, 753–773.
Eisma, D., Irion, G., 1988. Suspended matter and sediment transport. In: Salomons, W., Bayne, B.L., Duursma, E.K., Förstner, U. (Eds.), Pollution of the North Sea, An Assessment. Springer, Berlin, pp. 20–35.
Eisma, D., Kalf, J., 1987. Dispersal, concentration and deposition of suspended matter in the North Sea. Journal of the Geological Society (London) 144, 161–178.
Fält, L.-M., 1982. Late Quaternary sea-floor deposits off the Swedish west coast. PhD thesis, Chalmers University of Technology and University of Gothenburg. Publ A 37, 1–259.
Gjessing, J., 1980. The Aker moraines in southeast Norway. Norsk Geografisk Tidsskrift 34 (1), 9–34.
Gjessing, J., Spjeldnaes, N., 1979. Dating of the Grefsen moraine and remarks on the deglaciation of southeast Norway. Norsk Geografisk Tidsskrift 33 (2), 71–81.
Gyllencreutz, R., Jakobsson, M., Backman, J., 2005. Holocene sedimentation in the Skagerrak interpreted from chirp sonar and core data. Journal of Quaternary Science 20 (1), 21–32.
Hafsten, U., 1983. Shore-level changes in south Norway during the last 13,000 years, traced by biostratigraphical methods and radiometric datings. Norsk Geografisk Tidsskrift 37, 63–79.
Hass, H.C., 1996. Northern Europe climate variations during late Holocene: evidence from marine Skagerrak. Palaeogeography, Palaeoclimatology, Palaeoecology 123, 121–145.
Houmark-Nielsen, M., Kjaer, K.H., 2003. Southwest Scandinavia, 40–15 kyr BP: paleogeography and environmental change. Journal of Quaternary Science 18 (8), 769–786.
Jelgersma, S., 1979. Sea-level changes in the North Sea basin. In: Oerle, E., Shüttenhelm, R.T.E., Wiggers, A.J. (Eds.), The Quaternary History of the North Sea, Symposia Universitatis Upsaliensis Annum Quingentesimum Celebrantis, vol. 2, pp. 233–248.
Jiang, H., Björck, S., Knudsen, K.L., 1997. A palaeoclimatic and palaeoceanographic record of the last 11 000 14C years from the Skagerrak–Kattegat, northeastern Atlantic margin. The Holocene 7 (3), 301–310.
Klingberg, F., 1996. The late Weichselian–early Holocene Lindhov clay sequence in the Varberg area, southwestern Sweden. Geological Survey of Norway Bulletin 430, 17–24.
Klitgaard-Kristensen, D., Sejrup, H.P., Haflidason, H., 2001. The last 18 kyr fluctuations in Norwegian Sea surface conditions and implications for the magnitude of climatic change: evidence from the North Sea. Paleoceanography 5 (16), 455–467.
Knudsen, K.L., Conradsen, K., Heier-Nielsen, S., Seidenkrantz, M.-S., 1996. Quaternary palaeoceanography and palaeogeography in northern Denmark: a review of the results from the Skagen cores. Bulletin of the Geological Society of Denmark 43, 22–31.
Kranck, K., 1975. Sediment deposition from flocculated suspensions. Sedimentology 22, 111–123.
Kranck, K., 1981. Particulate matter grain-size characteristics and flocculation in a partially mixed estuary. Sedimentology 28, 107–114.
Kranck, K., 1987. Granulometric changes in fluvial sediments from source to deposition. Mitteilungen aus dem Geologisch-Paläontologischen Institut der Universität Hamburg 64, 45–56.
Krank, K., Milligan, T.G., 1985. Origin of grain size spectra of suspension deposited sediment. Geo-Marine Letters 65 (5), 61–66.
Kranck, K., Milligan, T.G., 1991. Grain size in oceanography. In: Syvitski, J.P.M. (Ed.), Principles, Methods and Application of Particle Size Analysis. Cambridge University Press, New York, USA, pp. 332–345.
Kuijpers, A., Dennegård, B., Albinsson, Y., Jensen, A., 1993. Sediment transport pathways in the Skagerrak and Kattegat as indicated by sediment Chernobyl radioactivity and heavy metal concentrations. Marine Geology 111, 231–244.
Labeyrie, L., Cortijo, E., Jansen, E., Shipboard Scientific Party, 2003. MD114/IMAGES V cruise report. Institut Polaire Francais Paul-Émile Victor (IPEV), les rapports de campagnes à la mer OCE/2003/02, 1–850.
Lagerlund, E., Houmark-Nielsen, M., 1993. Timing and pattern of the last deglaciation in the Kattegat region, southwest Scandinavia. Boreas 22, 337–347.
Lambeck, K., 1995. Late Devensian and Holocene shorelines of the British Isles and North Sea from models of glacio-hydro-isostatic rebound. Journal of the Geological Society (London) 152, 437–448.
Lambeck, K., 1999. Shoreline displacements in southern–central Sweden and the evolution of the Baltic Sea since the last maximum glaciation. Journal of the Geological Society (London) 156, 465–486.
Leth, J.O., 1996. Late Quaternary geological development of the Jutland Bank and the initiation of the Jutland Current, NE North Sea. Geological Survey of Norway Bulletin 430, 25–34.
Liebezeit, G., van Weering, T.C.E., Rumohr, J. (Eds.), 1993. Special Issue: Holocene Sedimentation in the Skagerrak, Marine Geology, vol. 111, pp. 189–379.
Longva, O., Bakkejord, K.J., 1990. Iceberg deformation and erosion in soft sediments, southeast Norway. Marine Geology 92 (1–2), 87–104.
Longva, O., Thoresen, M.K., 1991. Iceberg scours, iceberg gravity craters and current erosion marks from a gigantic Proboreal flood in southeastern Norway. Boreas 20 (1), 47–62.
Longva, O., Thorsnes, T. (Eds.), 1997. Skagerrak in the Past and at the Present—An Integrated Study of Geology, Chemistry, Hydrography and Microfossil Ecology. Geological Survey of Norway Special Publication, vol. 8, pp. 1–100.
Lundqvist, J., Wohlfarth, B., 2001. Timing and east–west correlation of south Swedish ice marginal lines during the late Weichselian. Quaternary Science Reviews 20, 1127–1148.
McCave, I.N., Manighetti, B., Robinson, S.G., 1995. Sortable silt and fine sediment size/composition slicing: parameters for

paleocurrent speed and paleoceanography. Paleoceanography 10 (3), 593–610.
Mörner, N.-A., 1979. The deglaciation of Sweden: a multi-parameter consideration. Boreas 8, 189–198.
Nordberg, K., 1991. Oceanography in the Kattegat and Skagerrak over the past 8000 years. Paleoceanography 4 (6), 461–484.
Nordberg, K., Bergsten, H., 1988. Biostratigraphic and sedimentological evidence of hydrographic changes in the Kattegat during the later part of the Holocene. Marine Geology 83, 135–158.
North Sea Task Force, 1993. North Sea Quality Status Report 1993. Oslo and Paris Commisions, London. Olsen and Olsen, Fredensborg, 1–132.
Ottesen, D., Bøe, R., Longva, O., Olsen, H.A., Rise, L., Skilbrei, J.R., Thorsnes, T., 1997. Geologisk atlas-Skagerrak. Atlas over kvartaere avsetninger, bunnsedimenter, berggrunn og batymetri i norsk sektor av Skagerrak. Geological Survey of Norway-Rapport 96, 1–138 (in Norwegian with English summary).
Otto, L., Zimmerman, T.F., Furnes, G.K., Mork, M., Saetre, R., Becker, G., 1990. Review of the physical oceanography of the North Sea. Netherlands Journal of Sea Research 26 (2–4), 161–238.
Pederstad, K., Roaldset, E., Rønningsland, T.M., 1993. Sedimentation and environmental conditions in the inner Skagerrak–outer Oslofjord. Marine Geology 111, 245–268.
Petersen, K.S., 2004. Late Quaternary environmental changes recorded in the Danish marine molluscan faunas. Geologic Survey of Denmark and Greenland Bulletin 3, 258–259.
Rodhe, J., 1987. The large-scale circulation in the Skagerrak; interpretation of some observations. Tellus 39A, 245–253.
Rodhe, J., 1996. On the dynamics of the large-scale circulation of the Skagerrak. Journal of Sea Research 35 (1–3), 9–21.
Rodhe, J., 1998. The Baltic and North Seas: a process-oriented review of the physical oceanography. In: Robinson, A.R., Brink, K.H. (Eds.), The Sea, vol. 11. John Wiley and Sons, New York, pp. 699–732.
Rodhe, J., Holt, N., 1996. Observations of the transport of suspended matter into the Skagerrak along the western and northern coast of Jutland. Journal of Sea Research 35 (1–3), 91–98.
Senneset L. 2002. A record of high resolution ocean variability from Skagerrak over the past 900 years. Masters thesis, Department of Geology, University of Bergen, Norway, 1–58.
Smith, W.H.F., Sandwell, D.T., 1997. Global sea floor topography from satellite altimetry and ship depth soundings. Science 5334 (277), 1956–1962.
Sørensen, R., 1979. Late Weichselian deglaciation in the Oslofjord area, south Norway. Boreas 8, 241–246.
Sørensen, R., 1992. The physical environment of late Weichselian deglaciation of the Olsofjord region, southeastern Norway. Geological Survey of Sweden, Ca 81, 339–346.
Stabell, B., Thiede, J. (Eds.), 1985. Upper Quaternary Marine Skagerrak (NE North Sea) Deposits: Stratigraphy and Depositional Environment, Norsk Geologisk Tidsskrift, vol. 65 (1–2), pp. 1–149.
Stabell, B., Thiede, J., 1986. Paleobathymetry and paleogeography of southern Scandinavia in the late Quaternary. Meyniana 38, 43–59.
Stabell, B., Werner, F., Thiede, J., 1985. Late Quaternary and modern sediments of the Skagerrak and their depositional environment: an introduction. Norsk Geologisk Tidsskrift 65, 9–17.
Stevens, R., Bengtsson, H., Lepland, A., 1996. Textural provinces and transport interpretations with fine-grained sediments in the Skagerrak. Journal of Sea Research 35 (1–3), 99–110.
Stuiver, M., Braziunas, T.F., 1993. Modelling atmospheric 14C influences and 14C ages of marine samples to 10 000 BC. Radiocarbon 35 (1), 137–189.
Stuiver, M., Reimer, P.J., 1993. Extended 14C data base and revised CALIB 3.0 14C age calibration program. Radiocarbon 35 (1), 215–230.
Stuiver, M., Reimer, P.J., Bard, E., Beck, J.W., Burr, G.S., Hughen, K.A., Kromer, B., McCormac, G., van der Plicht, J., Spurk, M., 1998a. INTCAL98 radiocarbon age calibration, 24,000–0 cal BP. Radiocarbon 40, 1041–1083.
Stuiver, M., Reimer, P.J., Braziunas, T.F., 1998b. High-precision radiocarbon age calibration for terrestrial and marine samples. Radiocarbon 40, 1127–1151.
Svansson, A., 1975. Physical and chemical oceanography of the Skagerrak and Kattegat: I. Open sea conditions. Report, vol. 1. Fishery Board of Sweden, Institute of Marine Research, pp. 1–88.
Telford, R.J., Heegard, E., Birks, H.J.B., 2004. The intercept is a poorly behaved estimate of a calibrated radiocarbon age. The Holocene 14 (2), 296–298.
Thiede, J., 1987. The late Quaternary Skagerrak and its depositional environment. Boreas 16 (4), 425–432.
van Leussen, W., 1994. Estuarine macroflocs and their role in fine-grained sediment transport. Doctoral thesis, University of Utrecht, 488 pp.
van Weering, T.C.E., 1981. Recent sediments and sediment transport in the northern North Sea; surface sediments of the Skagerrak. In: Nio, S.-D., Schöttenhelm, R.T.E., van Weering, T.C.E. (Eds.), Holocene Marine Sedimentation in the North Sea basin. Special Publication of the International Association of Sedimentologists, vol. 5, pp. 335–359.
van Weering, T.C.E., 1982a. Shallow seismic and acoustic reflection profiles from the Skagerrak; implications for recent sedimentation. Proceedings of the Koninklijke Nederlandse Akademie van Wetenschappen. Series B 85 (2), 129–154.
van Weering, T.C.E., 1982b. Recent sediments and sediment transport in the northern North Sea; pistoncores from Skagerrak. Proceedings of the Koninklijke Nederlandse Akademie van Wetenschappen. Series B 85 (2), 155–201.
van Weering, T.C.E., Berger, G.W., Kalf, J., 1987. Recent sediment accumulation in the Skagerrak, northeastern North Sea. Netherlands Journal of Sea Research 21, 177–189.
van Weering, T.C.E., Berger, G.W., Okkels, E., 1993. Sediment transport, resuspension and accumulation rates in the northeastern Skagerrak. Marine Geology 111, 269–285.
Werner, F., 1985. Sedimentary structures and the record of trace fossils in upper Quaternary marine Skagerrak deposits. Norsk Geologisk Tidsskrift 65 (1–2), 65–71.